



UNIVERSIDAD DE MALAGA

Tesis Doctoral por Compendio de Publicaciones

ESTUDIOS DE PROPAGACIÓN DE GRIETAS MEDIANTE CORRELACIÓN DE IMÁGENES Y MECÁNICA DE LA FRACTURA


Mehdi Mokhtarishirazabad

Málaga, May 2019



UNIVERSIDAD
DE MÁLAGA

AUTOR: Mehdi Mokhtarishirazabad

 <http://orcid.org/0000-0002-5035-0397>

EDITA: Publicaciones y Divulgación Científica. Universidad de Málaga



Esta obra está bajo una licencia de Creative Commons Reconocimiento-NoComercial-SinObraDerivada 4.0 Internacional:

<http://creativecommons.org/licenses/by-nc-nd/4.0/legalcode>

Cualquier parte de esta obra se puede reproducir sin autorización
pero con el reconocimiento y atribución de los autores.

No se puede hacer uso comercial de la obra y no se puede alterar, transformar o hacer obras derivadas.

Esta Tesis Doctoral está depositada en el Repositorio Institucional de la Universidad de Málaga (RIUMA): riuma.uma.es



UNIVERSIDAD DE MÁLAGA

Departamento de Ingeniería Civil, de Materiales y Fabricación

Tesis Doctoral por Compendio de Publicaciones

ESTUDIOS DE PROPAGACIÓN DE GRIETAS MEDIANTE CORRELACIÓN DE IMÁGENES Y MECÁNICA DE LA FRACTURA

MULTI-PARAMETER FRACTURE MECHANICS ANALYSIS OF FATIGUE CRACK PROPAGATION BY DIGITAL IMAGE CORRELATION

Autor:

MEHDI MOKHTARISHIRAZABAD

Ingeniero de Materiales- Metalurgia Industrial por la Universidad Ferdowsi de
Mashhad, Irán

Director:

D. PABLO LÓPEZ CRESPO

Tesis doctoral presentada en la
ESCUELA DE INGENIERÍAS INDUSTRIALES de la UNIVERSIDAD DE
MÁLAGA

para la obtención del Grado de Doctor

Málaga, Mayo de 2019

D. Pablo López Crespo, Doctor del Área de Ciencia de Materiales e Ingeniería Metalúrgica, de la Universidad de Málaga, como Director de la Tesis Doctoral.

“ESTUDIOS DE PROPAGACIÓN DE GRIETAS MEDIANTE CORRELACIÓN DE IMÁGENES Y MECÁNICA DE LA FRACTURA”

Presentada por D. Mehdi Mokhtarishirazabad en la ESCUELA DE INGENIERÍAS INDUSTRIALES de la UNIVERSIDAD DE MÁLAGA para la obtención del Grado de Doctor.

Hace constar que dicha tesis queda avalada por los siguientes artículos de investigación:

1. M. Mokhtarishirazabad, P. Lopez-Crespo, B. Moreno, A. Lopez-Moreno, M. Zanganeh, Evaluation of crack-tip fields from DIC data: A parametric study, International Journal of Fatigue, Volume 89, 2016, Pages 11-19.
2. M. Mokhtarishirazabad, P. Lopez-Crespo, B. Moreno, A. Lopez-Moreno, M. Zanganeh, Optical and analytical investigation of overloads in biaxial fatigue cracks, International Journal of Fatigue, Volume 100, Part 2, 2017, Pages 583-590.
3. Mokhtarishirazabad M, Lopez-Crespo P, Zanganeh M. Stress intensity factor monitoring under cyclic loading by digital image correlation, Fatigue & Fracture of Engineering Materials and Structures, Volume 41, 2018; Pages 2162–2171.

En Málaga, a de de 2019

Fdo: Pablo López Crespo

Director

Fdo: Belén Moreno

Morales

Tutora

To my parents, Mokhtar and Fatemeh

Resumen

La evaluación precisa de los parámetros de fractura es crucial para estimar el comportamiento de los componentes mecánicos en condiciones de servicio. Las distintas técnicas experimentales son de gran utilidad para mejorar las predicciones y los análisis de integridad estructural en los materiales. El factor de intensidad de tensiones (SIF por sus siglas en inglés) es un parámetro comúnmente usado para estudiar la propagación de grietas de fatiga en órganos que trabajan en régimen eminentemente lineal elástico. Por esta razón, existen numerosos grupos de investigación dedicados al desarrollo de métodos experimentales, numéricos y analíticos para mejorar las estimaciones del SIF para distintas condiciones de carga y distintas geometrías. Correlación de imágenes (DIC por sus siglas en inglés) es una herramienta relativamente simple y de gran versatilidad que permite medir campos completos de desplazamientos o deformaciones en objetos sometidos a cargas. La combinación de datos obtenidos experimentalmente con soluciones analíticas como los modelos de Westergaard, Muskhilishvili o Williams, permite la estimación de los valores del SIF en muy diversos casos. Sin embargo, aspectos como la selección más idónea de parámetros experimentales o las limitaciones de esta técnica siguen generando muchas dudas en la comunidad científica. Este trabajo se centra principalmente en tres aspectos: la optimización de los parámetros experimentales de DIC para la evaluación del SIF, la medición continua del SIF mediante DIC y el estudio del comportamiento en condiciones de carga complejas (carga biaxial) con y sin la presencia de cierre de grieta. A tal efecto se ha empleado un método multi-puntos sobredeterminado que aúna la elegancia y simplicidad de los modelos elásticos con la extracción de información real del comportamiento del material en su superficie. En este caso hemos optado por el modelo elástico basado en el desarrollo en series de Williams y la medida experimental de datos en torno al vértice de la grieta se ha realizado mediante DIC. En la etapa de optimización se examinan diferentes parámetros, como el número de términos en la serie de Williams, el tamaño del campo de visión y la ubicación óptima del área de interés. El efecto de estos parámetros en la evaluación de SIF se examina y optimiza con el objetivo de mejorar la precisión en los valores del SIF, así como mejorar la estabilidad de la metodología. Con los parámetros obtenidos se observa una gran estabilidad para la evaluación continua del SIF tanto para cargas estáticas como para cargas cíclicas. Se ha estudiado también un caso de mayor complejidad pero a su vez mayor utilidad desde el punto de vista industrial como es la

aplicación de cargas biaxiales. Los resultados mostraron una buena concordancia entre las soluciones experimentales y las analíticas. Por último, en semejantes condiciones, se ha podido detectar la presencia de fenómenos de cierre de grieta en fatiga, demostrando de este modo la utilidad de estas investigaciones en condiciones de cargas variables.

Abstract

Accurate evaluation of the fracture parameters is crucial for estimating the behaviour of the mechanical components in service condition. Experimental observations are extremely useful to provide accurate and reliable information for modern structural integrity analysis. The stress intensity factor (SIF) is a key parameter for understanding the fatigue crack propagation behaviour of structures prone to linear elastic failure. The SIF has been widely studied and a number of experimental, numerical and analytical methods have been developed and continue being developed to improve the estimation of the SIF for different loading conditions and component geometries. Digital Image Correlation (DIC) is a simple and versatile method for full-field quantification and can be used to measure experimentally the displacement data from a surface of a component being strained. By combining the experimentally evaluated displacement data with analytical solutions such as Westergard's, Muskhilishvili's and Williams' series, one is able to evaluate the SIF in cracked components. However, the selection of the experimental parameters and the limitations of the approach (e.g. the maximum permitted plasticity at the crack tip) are still a controversial concept. This work concentrates on three main topics: optimization the experimental DIC parameters for SIF evaluation, continuous measurement of SIF by DIC and evaluation of crack tip field under complex loading conditions (biaxial loading) with and without the presence of overloads. A multipoint over-deterministic method is employed to combine an elastic model based on Williams' solution for displacement distribution around the crack tip with the experimentally full field measurement of displacement at the crack tip by DIC. Different parameters such as number of terms in Williams' series, size of the field of view and the best location of the area of interest are examined in the optimisation stage. The effect of these parameters on the SIF evaluation are then tested for stable and accurate SIF estimation. The method showed a great stability for continuous evaluation of SIF under static and cyclic loads. It was also successfully applied on cylindrical samples under biaxial loading and the results showed good agreement between analytical and experimental evaluation of SIF. Finally, the methodology was also employed successfully to detect crack closure effects.

Acknowledgements

I would like to express my sincere gratitude to my supervisor Dr Pablo Lopez-Crespo for all scientific and personal supports during my PhD studies. My sincere thanks to Professor Belen Moreno for her invaluable advices in different parts of this scientific endeavour. I would also like to thank Dr Mohammad Zanganeh, from NASA Johnson Space Centre, USA, for the industrial support, Dr Kristin Hockauf from Chemnitz University of Technology, Germany and Dr Mahmoud Mostafavi from the University of Bristol, UK, for hosting me during the scientific visits that I conducted in their labs. Financial support from Junta de Andalucía through Proyectos de Excelencia grant reference TEP-3244, the University of Malaga and Campus de Excelencia Internacional del Mar (CEIMAR) through Lineas Emergentes program and for providing PhD scholarship and Ministerio de Economia y Competitividad through grant reference MAT2016-76951-C2-2-P is greatly acknowledged. Last but not least, I highly appreciate the continuous support, encourage and understanding of my family, friends and colleagues during the last four years.

Contents

1. Introduction	1
2. Literature review	3
2.1. Fatigue of materials.....	3
2.2. Fatigue crack closure	6
2.3. Digital Image Correlation	7
2.4. Multi parameters fracture mechanics.....	9
2.5. DIC parameters affecting the estimation of K	10
2.6. Continuous measurement of SIF under cyclic loading by DIC	12
2.7. Capturing complex load history by DIC	14
3. Methodology	15
3.1. Optimizing DIC parameters for SIF measurement	15
3.2. SIF monitoring by DIC	19
3.3. Biaxial experiment.....	20
4. Results and discussion.....	26
4.1. Optimizing DIC parameters for SIF measurement	26
4.2. SIF monitoring by DIC	28
4.3. Biaxial experiment.....	30
5. Conclusions.....	33
References.....	35

List of Figures

Figure 1. Different modes of loading, a) Mode I (Tensile opening), b) Mode II (in-plane sliding), and c) Mode III (Anti-plane shear) [2].	4
Figure 2. Definition of coordinate axis ahead of a sharp crack tip in linear elastic isotropic body subjected to mode I of loading [12].	5
Figure 3. Evolution of plastic zone at crack wake by propagating a fatigue crack [2].	7
Figure 4. Schematic diagram of typical 2D DIC equipment [21].	8
Figure 5. An example of a speckle pattern applied with spray paint on a CT sample.	8
Figure 6. Concept of DIC [21].	9
Figure 7. Geometry of the CT specimen in accordance with ASTM standard [73].	16
Figure 8. Imaging configuration for DIC.	16
Figure 9. The difference between FOV and AOI. The FOV is the size of the whole image. Six different AOIs are defined within the FOV when $\lambda = 50\%$.	19
Figure 10. Schematic of loading sequences.	20
Figure 11. The microstructure of St52-3N steel. Black and white vertical bands are showing the pearlite and ferrite bands, respectively [79].	21
Figure 12. The geometry of the hollow cylinder specimen with a central hole. All dimensions are in mm.	21
Figure 13. The position of virtual extensometers for COD examination. The white bold mark shows the crack-tip position.	22
Figure 14. Evolution of crack length versus number of cycles for samples with and without OL cycle, a) samples S1 and S2 under higher cyclic loads, b) samples S3 and S4 under lower cyclic loads.	23
Figure 15. Crack growth rate as a function of the crack length for high (a) and low (b) baseline cyclic load.	24

Figure 16. The position of the AOI for deriving the displacement field ahead of a crack with the length of 0.669 mm after 53500 cycles (sample S2). The image has been rotated, so that the crack line becomes horizontal.	25
Figure 17. The behaviour of δ as a function of λ for different FOVs. Nine terms in Williams' expansion were used in all cases.	26
Figure 18. Effect of reducing data points in an AOI of $4 \times 4 \text{ mm}^2$ where $\lambda = 25\%$. ϕ is defined as the number of data points used in the analysis divided by the number of terms in the series. Note the logarithmic scale in ϕ scale.	27
Figure 19. Evolution of δ by increasing ΔK_{nom} for different sizes of AOI in mm.	29
Figure 20. Continuous evaluation of ΔK as a function of applied load at the last loading segment, leading to sudden fracture of the sample.	30
Figure 21. COD behaviour during loading and unloading cycle for different crack lengths of specimens. The number of cycles before and after OL where OL cycle was considered as 0 cycles, are shown in the graph b.	31

List of Tables

Table 1. Parameters used in previous works for estimating the SIF with DIC.....	12
Table 2. Mechanical properties of 2024-T351 Aluminum alloy [74].....	15
Table 3. Monotonic properties of St-52-3N steel [79].....	20
Table 4. Axial and shear stress values for specimens with and without OL cycle.	22
Table 5. Crack opening loads in a complete cycle.....	32
Table 6. Summary of the SIFs estimated for different samples and different crack lengths ...	32

1. Introduction

In modern designs, for the sake of structural integrity, accurate and reliable estimation of the fatigue strength of the structural materials is essential. It is well recognized that materials and structures contain cracks and flaws. Therefore, Fracture Mechanics approaches should be used for structural design and materials selections [1]. Although a number of parameters at a continuum level have been examined to correlate the crack propagation of flawed component, the most widely used fracture mechanics design parameter is the stress intensity factor (SIF). The SIF can completely characterizes the crack tip fields (stress, strain and displacement) in an ideally elastic material [1]. Apart from the conventional standard test methods for evaluating the SIF, it has been shown that crack-tip fields (strain, stress and displacement field) include essential information for accurate estimation of fracture parameters [2]. A number of different techniques are able to provide both surface and bulk information. Surface techniques include photo-elasticity [3], thermo-elasticity [4], Moiré interferometry [5] and digital image correlation (DIC) [6]. Bulk techniques include neutron diffraction [7] and X-ray diffraction [8]. Significant development in optical methodologies for evaluation of mechanical parameters from crack tip fields, has opened new doors toward engineers to have a more accurate estimation of fracture parameters of engineering component in service condition. Among full-field measurement techniques, DIC is widely used due to several advantageous rather other methods. DIC is technically easy to implement, no sophisticated sample preparation is needed, and it is basically a scale-free method. In other words, it can measure on the scale ranging from a few meters [9] to micro-meters [10,11]. By fitting the experimental extracted full-field displacement data with available analytical solutions, such as Williams' solution for crack tip fields, an experimental stress intensity factor can be determined. It should take into consideration that there are several factors which can affect the accuracy and reliability of the estimated SIF. The first section of this study is allocated to optimization the experimental DIC parameters for evaluating the SIF with high accuracy.

In the next section of the thesis, DIC is used as a robust non-destructive technique for structural health monitoring. One of the main advantages of using DIC as a non-destructive testing (NDT) method, is the capability of the method to be combined with analytical solutions for monitoring the fracture parameters. That is to say, while conventional NDT methods such as infrared and thermal testing, acoustic emission, eddy current and ultrasonic have been successfully employed to monitor the defects size, DIC can be used to monitor the changes in fracture parameters (such as SIF)

without the knowledge of the crack length or applied load. This is a great advantage studying complex geometries when there is no available analytical solution and numerical solution is extremely time consuming. Therefore, the hybrid method developed in the earlier sections is employed for continuous measurement of stress intensity factor of a crack under cyclic loading.

To examine the capability of DIC for more complicated loading condition, crack tip field of a sample under biaxial loading is studied in the final stage of this research. Cracks in structures are generally subjected to mixed mode loading condition, while, for the sake of simplicity, most of works tend to focus more on the simpler but less realistic case of uniaxial loading [2]. Therefore, there are many uncertainties related to the load sequence effect that is now well-known and is not normally incorporated into the crack growth models. DIC is employed as versatile full-field optical technique in combination with analytical methodology to study overloads in fatigue cracks under biaxial loading (tension-torsion).

2. Literature review

2.1. Fatigue of materials

Since the first half of nineteenth century when the first research on fatigue of materials was published [2], a huge number of researches have been conducted to determine the different types and mechanisms of fatigue of material. Nowadays, it is well-known that the majority of the failure of engineering components (50%-90%) is due to fatigue fracture [2,12]. One of the most common definition for the fatigue phenomenon in materials is determined by ASTM [13] as follows:

“The process of progressive localized permanent structural change occurring in a material subjected to conditions that produce fluctuating stresses and strains at some point or points and that may culminate in cracks or complete fracture after a sufficient number of fluctuations”.

As it can be seen from the above-mentioned definition of the fatigue process, it is a localized process. That is to say, the fatigue damage occurs at local areas that experience high stress or strain. Another important keyword in the fatigue process definition is the word crack. In many safety critical parts in industry it is normally assumed that small crack-like defects (e.g. impurity, porosity, etc.) exists prior to initial use of the component. Keeping in mind that fatigue is a localized process and there is a crack which always lead to the final failure of the component, the crack tip fields seem to provide invaluable information for predicting the fatigue crack growth behaviour. To this end, Fracture Mechanics can be used as a tool to study the fatigue process. Linear Elastic Fracture Mechanics (LEFM) is one of the most common methods for analysing the fatigue process of materials provided that materials conditions during the loading are predominantly linear elastic. [1,12].

Irwin extended the Griffith's theory of brittle fracture to metals with small plastic deformation at the crack tip. To quantify the crack tip driving force, he employed the Stress Intensity Factor (SIF). The SIF is known as one of the most important fracture parameters for characterising the crack behaviour of the engineering components. Since 1957 when Irwin [14] formulated the SIF a considerable work has been done to improve our understanding on its importance in crack growth behaviour under static and cyclic loading [1,15]. Finite element method had been employed widely during last decades for detailed analysis of the crack tip fields (stress, strain, displacement) to evaluate the SIF and phenomenon such as crack closure

[16,17]. In addition, some mathematical models have been introduced describing the crack tip field. Westergaard [18] came up with a stress function describing the elastic stress distribution ahead of a crack. Williams then expanded his solution to take into account the yielding effect at the crack tip [19]. The stress field in a linear elastic cracked body subjected to external forces can be expressed as follows [1]:

$$\sigma_{ij} = \left(\frac{k}{\sqrt{r}}\right) f_{ij}(\theta) + \sum_{m=0}^{\infty} A_m r^{\frac{m}{2}} g_{ij}^{(m)}(\theta) \quad (1)$$

where σ_{ij} is the stress tensor, r and θ represent polar coordinate system (Fig. 2), k is a constant, and f_{ij} is a dimensionless function of θ in the first term. A_m is the amplitude and g_{ij} is a dimensionless function of the θ for the m th term. Since the leading term in the solution is proportional with $1/\sqrt{r}$, it approaches to infinity when $r \rightarrow 0$, while higher order terms remains finite or approach zero. That is, the stress near the crack tip is a function of $1/\sqrt{r}$. In Eq. 1, k can be replaced by SIF, K , where $K = k\sqrt{2\pi}$. For the sake of simplicity, the higher order terms are often ignored. However, it is essential to consider higher order terms to describe crack tip stress state accurately. For example, Larsson et al. [20] has shown that considering second non-singular term in Williams' series expansion can improve the evaluation of stress state ahead of a crack tip in plane strain conditions. Effect of considering higher order terms on the accuracy of the SIF estimation is examined in section 3.1.

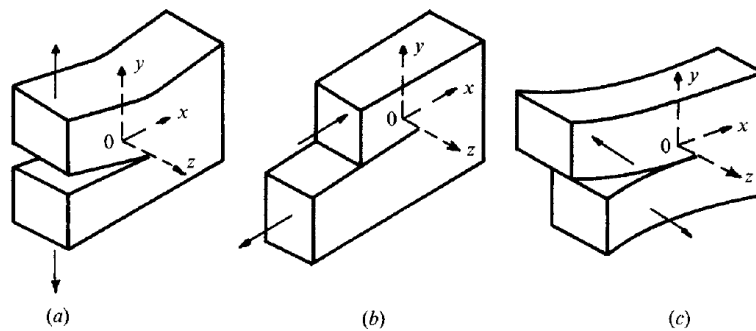


Figure 1. Different modes of loading, a) Mode I (Tensile opening), b) Mode II (in-plane sliding), and c) Mode III (Anti-plane shear) [2].

Fig. 1 shows three types of loading that can be applied to a crack including tensile opening (mode I), in-plane sliding (mode II), and out of plane shear (mode III). Fig. 2 illustrates the stress distribution ahead of a through-thickness sharp crack in linear elastic isotropic body subjected to mode I loading [12].

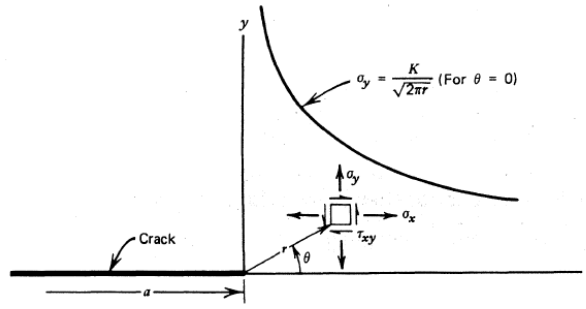


Figure 2. Definition of coordinate axis ahead of a sharp crack tip in linear elastic isotropic body subjected to mode I of loading [12].

The displacement field near the crack tip can also be described as follows [21]:

$$\begin{aligned} u &= \sum_{n=1}^{\infty} \frac{r^{\frac{n}{2}}}{2\mu} a_n \left\{ \left[\kappa + \frac{n}{2} + (-1)^n \right] \cos \frac{n\theta}{2} - \frac{n}{2} \cos \frac{(n-4)\theta}{2} \right\} \\ v &= \sum_{n=1}^{\infty} \frac{r^{\frac{n}{2}}}{2\mu} a_n \left\{ \left[\kappa - \frac{n}{2} - (-1)^n \right] \sin \frac{n\theta}{2} + \frac{n}{2} \sin \frac{(n-4)\theta}{2} \right\} \end{aligned} \quad (2)$$

where u and v are the horizontal and vertical displacement respectively. μ is the shear modulus and $\kappa = (3 - \nu)/(1 + \nu)$ for plane stress and $\kappa = 3 - 4\nu$ for plane strain condition, ν is the Poisson's ratio, r and θ are radial and phase distance from the crack, a and b are constant. It can be seen from Eq. 2 that by using a reverse solution, one is able to quantify the SIF if the state of crack tip field is known. For example, if by using an experimental method such as DIC, the state of the displacement field around the crack tip is determined, an experimental evaluation of SIF can be achieved.

Recently, Christopher et al. [22] introduced a new model for fatigue crack growth by including the K , T -stress, interfacial shear stresses, and a “retarding stress”. They claim that their model can identify the influence of stresses arising from plastic deformation [23] related to crack growth. All of the proposed models have been validated by experimental full-field data. Different techniques have been developed to obtain a full-field measurement of the crack tip field, experimentally, such as Moiré interferometry [5], photo-elasticity [3], thermo-elasticity [4], and DIC [6]. In section 3.3, DIC is introduced as a robust method for extracting the experimental full-field displacement data and its application for evaluating the widely used fracture parameters such as SIF is discussed.

2.2. Fatigue crack closure

The phenomenon in which the fatigue crack remains closed even after applying far-field tensile load, was observed and rationalised by Elber in 1970 [2]. This behaviour was attributed to elastic constraint of the material plastically stretched along the crack flanks by growing the crack. Plasticity-induced crack closure is the term coined for this type of the crack closure [2,24,25]. Residual plastic stretch at the crack wake is not the only source of crack closure [26]. Oxide induced crack closure, microscopic crack closure, viscous fluid-induced crack closure and transformation induced crack closure are the other types of crack closure. Elber's finding suggests that fatigue crack growth rate is not depend on only the crack tip condition but also depends on the state if the materials at the crack flanks behind the crack tip [27]. Therefore, for predicting the fatigue crack growth, the load history, length of the crack and stress state are playing important roles. Fig. 3 shows how the plastic wake develops for fatigue cracks with different crack length propagating under constant amplitude of tensile stresses .The effect of crack closure can lead a deviation from Paris' Law, which can be considered in the models by introducing $\Delta K_{eff} = K_{max} - K_{op}$, where K_{op} is the SIF when the crack is open fully [2,25]. A number of different methods have been developed for evaluating the K_{op} . In general, they can be divided in two main groups: direct methods such as optical and scanning electron microscopy observations, replica, etc, and indirect methods, in which the compliance changes during the loading cycles are measured, like back face strain and crack mouth opening displacement (CMOD) [28]. The load-displacement/strain data are then used to determine the opening load (P_{op}). Some of the most common methods are as follows:

- Deviation point from the linearity of the upper part of the load-displacement curve;
- 1% offset slope method;
- Deviation point from the linearity of the upper part of the load-differential displacement curve;
- The intersection point between two tangent lines, fitted to the upper and lower linear part of the load-displacement curve.

The advantages and disadvantages of each method is discussed in details by Stoychev and Kujawski [28].

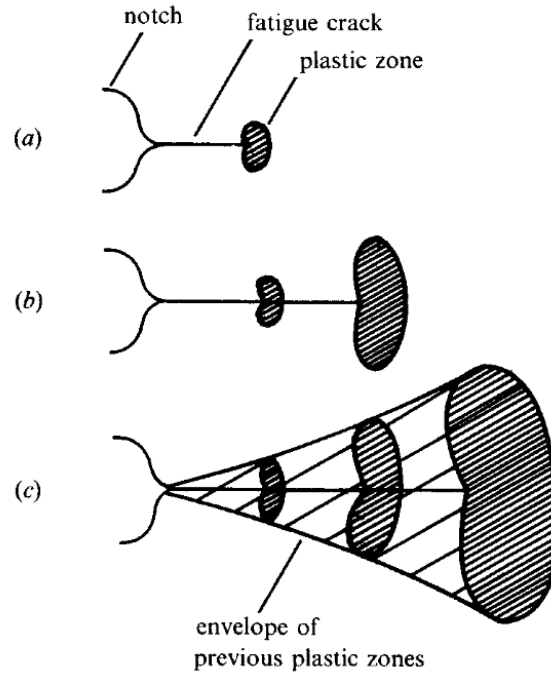


Figure 3. Evolution of plastic zone at crack wake by propagating a fatigue crack [2].

2.3. Digital Image Correlation

Since 1980s in which a group of researchers at the University of South Carolina [29] developed the DIC method for obtaining the full-field in-plane deformation of an object directly, a growing number of researches has been done to modify the method and its parameters. DIC is a straight forward, low cost and simple method to measure experimentally surface deformation data with few advantages compared to other full-field techniques such as Moiré interferometry, photo-elasticity and thermo-elasticity. A schematic diagram of a typical two-dimensional DIC is illustrated in Fig. 4.

In brief, DIC consists mainly of three sequences. First step is sample preparation which includes providing a grey scale random pattern called “speckle” on the surface of the sample. Fig. 4 shows an example of such speckle pattern.

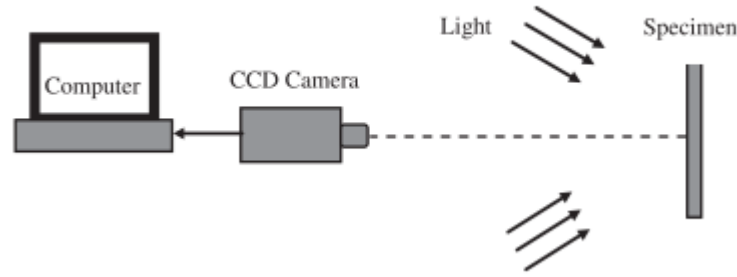


Figure 4. Schematic diagram of typical 2D DIC equipment [21]

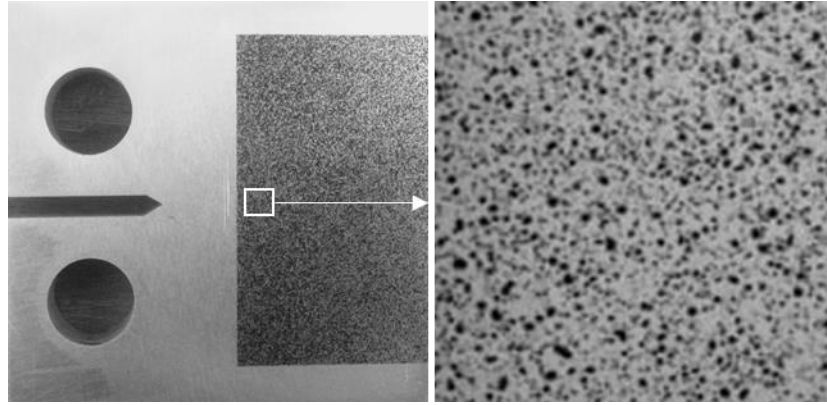


Figure 5. An example of a speckle pattern applied with spray paint on a CT sample.

This pattern can be achieved simply by spray painting the sample with white and black colours to obtain a random pattern of high contrast markers (Fig. 5). Next is taking digital images before and after loading from the surface of the specimen. Each image is made of pixels with distinct grey scale intensity. Finally, DIC uses correlation algorithm to track the markers on the pattern by comparing the first image (reference image), when no load is applying to the sample, with the deformed image taken during the loading. Since the intensity of a pixel in a digital image is not unique, in the correlation method, the image is divided to smaller windows called subset which is always made of an odd number of pixels. The pattern inside the subset is then correlated with the same subset in the reference image to calculate the displacement in the centre of the subset, point P. A Taylor expansion about the point P can be used to find the displacement of P from (x_0, y_0) to (x_1, y_1) , point P^* as follows :

$$x_1 = x_0 + u_0 + \frac{du}{dx} \Delta x + \frac{du}{dy} \Delta y + \frac{1}{2} \frac{d^2u}{dx^2} \Delta x^2 + \frac{1}{2} \frac{d^2u}{dy^2} \Delta y^2 + \frac{d^2u}{dxdy} \Delta x \Delta y \quad (3)$$

$$y_1 = y_0 + v_0 + \frac{dv}{dx} \Delta x + \frac{dv}{dy} \Delta y + \frac{1}{2} \frac{d^2v}{dx^2} \Delta x^2 + \frac{1}{2} \frac{d^2v}{dy^2} \Delta y^2 + \frac{d^2v}{dxdy} \Delta x \Delta y \quad (4)$$

where u_0 and v_0 are the horizontal and vertical displacement of point P, respectively, $\Delta x = x_1 - x_0$ and $\Delta y = y_1 - y_0$.

Higher order terms in Eqs. 3, and 4 are used to consider the subset rotation and distortion as shown in Fig. 6. The correlation between two subsets can be established in several methods which have their own pros and cons. For example, the correlation between the two subsets (before and after deformation) can be done by minimizing a correlation factor, C:

$$C = \frac{\sum_s [G(x_0, y_0) - H(x_1, y_1)]^2}{\sum_s G^2(x_0, y_0)} \quad (5)$$

where G and H are the grey scale light intensities corresponding to all points in the subset, S. This process performs for all subsets in the image. An overlap between neighbour subsets is set to have a sub-pixel accuracy. In this manner, a full field displacement of the area of interest (AOI) can be obtained.

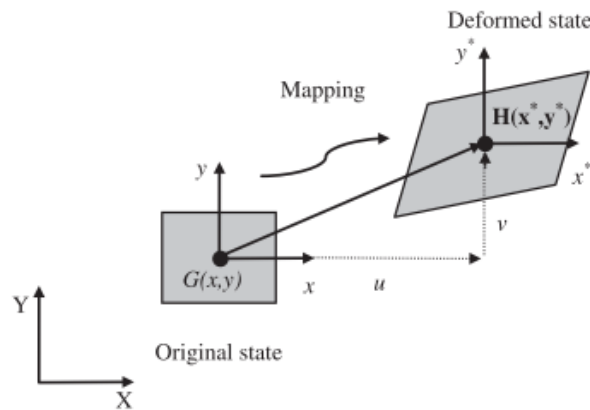


Figure 6. Concept of DIC [21]

The details of the method and algorithms are comprehensively described by Sutton et al. [16].

2.4. Multi parameters fracture mechanics

Based on classical fracture mechanics theories, a single parameter like K_I or J can characterise the stresses or strains near the crack tip under small scale yielding condition where the size of plastic zone is negligible comparing to the crack length and size of the body [1,30].

However, in the presence of excessive plasticity, single-parameter fracture mechanics is not valid anymore and fracture toughness becomes dependent on size and geometry of the sample. Higher order terms in Williams' infinite power series become more and more important at the presence of considerable crack tip plasticity. For example, second term in the Williams' series, known as T-stress, remains finite at the crack tip and it is independent of the distance from crack tip. It has been shown that T-stress has a considerable effect on the state of stresses and strains near the crack tip, as a result on the shape of plastic zone at the crack tip [1]. A number of studies have been conducted to evaluate the effect of higher order term on stress or strain state ahead of a crack tip. Utilising an over-deterministic least square method for evaluating mixed mode stress field parameters by the technique of photoelasticity, Ramesh et al. [3] showed the importance of using multi-parameter stress equations for solving real life problems where displacement data are collecting from a large area. They used the fringe order minimisation error as their convergence criteria. The method was tested in three different geometries and for those data, a minimum of 6 parameters were required to obtain a convergence error less than 0.1 in fringe order (N) in modes I and II.

Yoneyama et al. [31] suggested determining SIF by adopting the convergent values (considering more than 7 terms). A nonlinear least square method was used in their research for estimating SIF from displacement data provided by DIC from a FOV of $6 \times 5 \text{ mm}^2$. Abovementioned studies show the importance of considering higher order terms in determination of the state the crack tip fields. It is also true when the experimental displacement field is used for evaluation of K ahead of a crack, especially when data are collecting from larger area. Selecting a suitable number of terms for evaluation of SIF from experimental data is one of the concerns of this study.

2.5. DIC parameters affecting the estimation of K

Experimentally, DIC measurement accuracy can be affected by several factors, such as subpixel optimization algorithm, subset size, image quality, etc. [32]. It is evident that the more accurate displacement data, the more reliable estimation of SIFs. While the random error in any measurement is the inherent part of each measurement, systematic error is predictable and is typically constant and proportional to the true value [33]. Systematic errors in DIC as a result of intensity interpolation, overmatched and under-matched subset shape function have been explored by Schreier et al. [34,35] and Yu et al. [36]. A thorough study on the errors caused by

different bit depths of the image, image saturation in respect with subset size, speckle pattern and subset shape function on synthetic images has been conducted by Fazzini et al. [37]. It was shown that decreasing the encoding of the images and overexpose of the speckle deteriorate the measurements by a factor of 2 and 10 respectively. Pan [38] proposed a reliability-guided DIC method which is applicable to images with shadows, discontinuous areas, and deformation discontinuities. In optic literature, the size of the DIC image is studied through the field of view (FOV) and is defined as the angular extent for a given scene imaged by a camera [16]. Since the FOV determines the number and position of data points for a constant subset size, the FOV must be taken into consideration as key parameter for SIF evaluation from DIC data. A considerable discrepancy has been observed in the literature in evaluation of SIF using DIC method due to selecting different experimental or analytical parameters. For example, Vasco-Olmo et al. [39], evaluated the fatigue crack shielding by analysing displacement field data obtained by 2D DIC and utilizing four different models. They reported that the CJP model showed an extraordinary potential for the evaluation of the crack-tip shielding during fatigue crack growth. A finite element analysis of the stress field ahead of a cracked plate has been conducted by Berto and Lazzarin [40,41]. They were able to obtain good estimations of the stress field in a very small area ahead of the crack-tip ($r = 0.01$ mm) by using K_I , K_{II} and T-stress in Williams' solution. In addition, they were also able to describe the stress field in larger areas by considering the first 7 terms in the series. Dehnavi et al. [42] estimated the SIF of a polycarbonate plate by DIC method (subset of 21×21 pixels) considering 4 terms of Williams' series taking a similar approach to Berto and Lazzarin.

The differences between all works above mentioned suggest that there exists a number of parameters that can influence the SIF estimations. These include the magnification factor, the FOV, the subset size, the dimensions of the AOI, the portion of crack included in the AOI, the masking of the crack-tip plastic zone and the number of terms considered in the analytical solution. Table 1 summarises the parameters that have been used in some of the most relevant works that estimated SIF from DIC.

Table 1 shows a clear discrepancy in the parameter selection for different works. Authors provided little or no justification for employing different parameters in the previous published work. Therefore, in the first attempt, the influence of the different parameters involved in estimating the SIF with DIC technique is studied in a structured way.

Table 1. Parameters used in previous works for estimating the SIF with DIC

Author	FOV (mm ²)	Crack portion inside AOI (λ)	Subset size (pixel)	Excluding plastic zone	No. of higher order terms
Peters et al. [43]	8	crack included	not-mentioned	not mentioned	convergence value
McNeill et al. [6]	12.7 \times 12.7	65%	not mentioned	No	up to 48 terms
Yoneyama et al. [31]	6 \times 5	50%	not mentioned	No	up to 10 terms
Hamam et al. [44] and Roux et al. [45]	2 \times 2	65% and 45%	12	Yes	sub/super singular terms
Yusof et al. [46]	\sim 12	50%	12	Yes	Muskhilishvili's app.
Lopez-Crespo et al. [47]	18 \times 24	50%	32	Yes	Muskhilishvili's app.
Yates et al. [21]	22 \times 16	30%	not mentioned	No	up to 15 terms
Dehnavi et al. [42]	not-mentioned	30%	21	Yes	4 terms

2.6. Continuous measurement of SIF under cyclic loading by DIC

In the second part of this study, after optimizing the DIC parameters for evaluation of SIF, the capability of this technique is examined for continuous measurement of the SIF on a sample under cyclic loading. In this manner, DIC perceived as a non-destructive testing (NDT) method for structural health monitoring. The accuracy for structural health monitoring has been vastly improved over the last few decades thanks to the development and improvement of a wide range of techniques for monitoring the crack (damage) initiation and growth in engineering structures. Among these, NDT techniques have been extremely useful for crack monitoring. Infrared and thermal testing [48], acoustic emission [49], eddy current [50,51] and ultrasonic [52,53] are among the most popular NDT techniques for monitoring the defect size. In addition, some efforts were aimed at improving the accuracy of these techniques by combining two or more of these techniques. For example, DIC has been coupled with acoustic emission technique to determine the critical stage of deformation mechanism at the onset of the plasticity of AZ31 Mg alloy [54]. Nevertheless, most of these methods have some disadvantages that make them difficult to be adapted for industrial environments such as being very expensive and limited application to a narrow range of materials and type of defects to be detected. For example, in ultrasonic method the accuracy is highly dependent on the operator skills and it is not suitable for detecting short cracks [55]. The application of eddy current method is also limited to electrically conductive materials and interpretation of complex signals requires a highly skilled operator [56]. Due to the nature of the signal source, acoustic emission method is not perfectly reproducible and it is not capable of detecting elastic deformation [57].

While the previously described methods are used to determine the crack geometry and length, accurate damage assessment of engineering structures subjected to changing loads often requires fracture parameters of the component to be evaluated. To this end, full field techniques such as DIC [6] have been developed to characterise crack tip fields in terms of strain, stress and displacement. As it was mentioned in the previous section, SIF is a key parameter for fatigue life prediction of engineering components prone to linear elastic failure. The prominent advantage of using the crack tip fields for evaluating SIF is that no previous knowledge of crack length, applied force or specimen geometry is needed. This makes it very suitable for characterisation of in-service engineering components [58]. DIC has been employed [47] to study the effect of crack closure and crack tip plasticity in the evaluation of SIF for specimens under different mixed-mode loads (I+II). Very promising results were obtained in early studies while estimating the SIF with DIC on C-specimens and three-point-bend specimens [6]. Improvement in digital photography allowed higher resolution images that improved the accuracy in estimating the SIF both under pure mode I and a range of mixed-mode conditions [31]. Edge-finding routines for locating the crack tip were subsequently incorporated to the program to automate the evaluation of SIF with DIC displacement data [59]. The crack-tip location was also evaluated from displacement fields with a number of numerical procedures, including reflective Newton method, Nelder-Mead Simplex method, genetic algorithm and Pattern Search method [60]. DIC also allowed other forms of crack evaluation through different parameters. For example, T-stress and crack tip opening angle were evaluated on double cantilever specimens made of 7010-T7651 aluminium alloy [21]. Elastic plastic crack assessment was achieved with different methodologies. The J-integral was estimated from a combination of DIC and finite element method displacements by applying the path and domain integral methods on annealed and unannealed pure aluminium A1050 [61]. Crack opening displacement (COD) measurements obtained with high magnification DIC were used to evaluate crack growth and closure mechanisms for different thicknesses on 6082-T6 aluminium alloy [62]. The plastic zone ahead of the crack [63] as a way to control the rate of crack growth was assessed with DIC on specimens with artificial cracks [64] and on specimens with real fatigue cracks [65]. To examine the capability of the proposed hybrid method, in the second part of this study, for the first time, a DIC methodology is used for continuous monitoring of the effective SIF under a range of different cyclic levels [66].

2.7. Capturing complex load history by DIC

While fracture problems can be simplified by considering mode I loading, cracks in structural materials are generally under mixed-mode loading condition [2]. Therefore, estimation of the fracture parameters based on mixed-mode loading condition will be more representative of the material fracture behaviour under the actual working condition. Different optical methods have been used for obtaining full-field information required for mixed-mode loading analysis previously. Sanford and Dally [67] have determined the mixed-mode SIFs by utilising isochromatic fringes near the crack-tip. They have reported that employing an over-deterministic approach on the data points provided by the full-field fringe patterns led to a highly accurate SIF estimation. Displacement fields derived by DIC technique have been utilised by Yoneyama et al. [31] to evaluate the mixed-mode SIFs of a polymer (polymethylmethacrylate). While they used a non-linear least square method for their solutions, Réthoré et al. [68] have developed a method based on the Lagrangian conservation law for mixed-mode SIFs estimations. A good agreement between analytical displacement fields generated based on the Muskhilishvili's complex function approach and the experimentally measured displacement fields (obtained by DIC) has been also reported by Lopez-Crespo et al [69]. The combined effect of overload (OL) and biaxial loading has been studied by potential drop technique [70].

Full-field optical techniques are very advantageous compared to other more traditional techniques. They are very versatile and can be used to study a wide range of aspects related to the OL, including evaluation of the plastic region, changes in the stress field due to the OL or experimental estimation of fracture mechanics parameters. Nevertheless, as it is described previously, they have been mostly applied to the uniaxial problem. In reality, most mechanical components are subjected to complex loading conditions with varying magnitude and direction. Therefore, it is desirable to apply full-field optical techniques to more complex loading conditions. In the last part of this work, a comprehensive optical and analytical methodology is used to study overloads [71] in fatigue cracks under biaxial loading. Most experimental information is extracted from full-field DIC data. Specimens with and without overloads are compared in terms of crack growth rate, COD and SIF [72].

3. Methodology

The experimental part of the work is explained in detail in ANNEXES I-III. Hereafter, only a summary of each experiment is presented. In general, all experiments were included taking images of a sample under cyclic loading following the post processing of the images for extracting the displacement field near the crack tip using the commercial software VIC-2D. The displacement data were then analysed using the routine used by Yates et al [21] to calculate an experimental SIF. The displacement data near the crack wake were also used for measuring the COD which were consequently used for measuring the opening load and effective SIF. Crack tip location were identified directly from the images at maximum load in each cycle using high magnification lenses.

3.1. Optimizing DIC parameters for SIF measurement

The uniaxial cyclic loading was applied on CT specimens which were extracted and machined in T-L direction (crack propagation along rolling direction) from a 2024-T351 aluminium alloy plate according to ASTM E-647 [73]. Fig. 7 illustrates the specimen geometry and dimensions. The mechanical properties of the material are summarised in Table 2. The sample surface was scratched with abrasive SiC sand paper to obtain a random grey intensity distribution required for DIC technique. Cyclic loading was applied then with a 100kN Instron servo-hydraulic testing machine. The sample for parametrical study was pre-cracked under mode I load at a frequency of 10 Hz, a load ratio (R) of 0.1 and a stress intensity range (ΔK_I) of 8 MPa \sqrt{m} so that the crack length was 20.30 mm ($a/W = 0.40$). Displacements were then measured under $R = 0.3$ and $\Delta K_I = 11$ MPa \sqrt{m} . Small scale yielding conditions were met in all tests.

Table 2. Mechanical properties of 2024-T351 Aluminum alloy [74]

Young's modulus, GPa	Yield Stress, MPa	Ultimate Tensile Strength, MPa	Elongation at break, %	Brinell Hardness
73	325	470	20	137

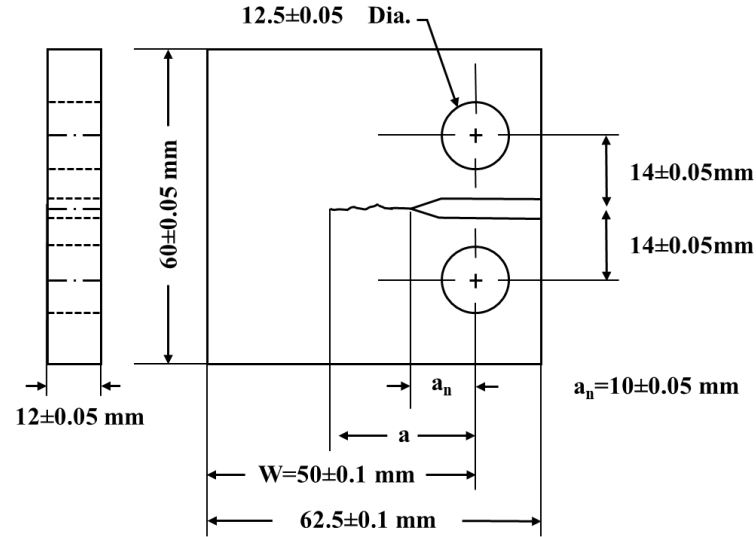


Figure 7. Geometry of the CT specimen in accordance with ASTM standard [73].



Figure 8. Imaging configuration for DIC.

An 8-bit 2452×2052 pixels CCD camera with the maximum frame rate at full resolution of 12 was used for taking images. Fields of view between $0.98 \times 0.82 \text{ mm}^2$ and $13.5 \times 11.3 \text{ mm}^2$ were imaged with a combination of a macro Navitar lens and an adaptor tube (see Fig. 8). In order to acquire a sufficient number of images (38 images per cycle), the loading rate was reduced to 0.1 Hz while capturing the images. Vic-Snap software [75] has been utilised for capturing the images and the corresponding applied load on the specimen for each image. Step size (the distance between two consecutive displacement vectors) was set to 1/4 of the subset size in order to achieve independent and non-repetitive data. A high-order interpolation scheme of optimized 8-tap spline was used to achieve sub-pixel accuracy. The correlation criterion was set to the zero-normalized sum of squared differences which is insensitive to offset and scale in lighting [16].

DIC test was done in different subset sizes ranging from 13 to 199 pixels for two different magnifications of $0.75\times$ and $0.35\times$. The obtained displacement data was then fitted into Williams' series [19]:

$$\text{Mode I} \begin{cases} u_I = \sum_{n=1}^{\infty} \frac{r^{\frac{n}{2}}}{2\mu} a_n \left\{ \left[\kappa + \frac{n}{2} + (-1)^n \right] \cos \frac{n\theta}{2} - \frac{n}{2} \cos \frac{(n-4)\theta}{2} \right\} \\ v_I = \sum_{n=1}^{\infty} \frac{r^{\frac{n}{2}}}{2\mu} a_n \left\{ \left[\kappa - \frac{n}{2} - (-1)^n \right] \sin \frac{n\theta}{2} + \frac{n}{2} \sin \frac{(n-4)\theta}{2} \right\} \end{cases} \quad (6)$$

$$\text{Mode II} \begin{cases} u_{II} = - \sum_{n=1}^{\infty} \frac{r^{\frac{n}{2}}}{2\mu} b_n \left\{ \left[\kappa + \frac{n}{2} + (-1)^n \right] \sin \frac{n\theta}{2} - \frac{n}{2} \sin \frac{(n-4)\theta}{2} \right\} \\ v_{II} = \sum_{n=1}^{\infty} \frac{r^{\frac{n}{2}}}{2\mu} b_n \left\{ \left[\kappa - \frac{n}{2} + (-1)^n \right] \cos \frac{n\theta}{2} + \frac{n}{2} \cos \frac{(n-4)\theta}{2} \right\} \end{cases} \quad (7)$$

where u and v are horizontal and vertical displacements in mode I and II, μ is the shear modulus and $\kappa = (3 - \nu)/(1 + \nu)$ for plane stress and $\kappa = 3 - 4\nu$ for plane strain condition, ν is the Poisson's ratio, r and θ are radial and phase distance from the crack, a_n are constants. Displacement field can be written in a matrix form by defining $f_{n,m}(r,\theta)$, $g_{n,m}(r,\theta)$, $h_{n,m}(r,\theta)$, and $l_{n,m}(r,\theta)$ as follows:

$$\begin{Bmatrix} u_1 \\ \vdots \\ u_m \\ v_1 \\ \vdots \\ v_m \end{Bmatrix} = \begin{bmatrix} f_{1,1} \cdots f_{n,1} & g_{1,1} \cdots g_{n,1} \\ \vdots & \vdots \\ f_{1,m} \cdots f_{n,m} & g_{1,m} \cdots g_{n,m} \\ h_{1,1} \cdots h_{n,1} & l_{1,1} \cdots l_{n,1} \\ \vdots & \vdots \\ h_{1,m} \cdots h_{n,m} & l_{1,m} \cdots l_{n,m} \end{bmatrix} \begin{Bmatrix} a_1 \\ \vdots \\ a_n \\ b_1 \\ \vdots \\ b_m \end{Bmatrix} \quad (8)$$

$$\begin{aligned} f_{n,m} &= \frac{r_m^{\frac{n}{2}}}{2\mu} \left\{ \left[\kappa + \frac{n}{2} + (-1)^n \right] \cos \frac{n\theta_m}{2} - \frac{n}{2} \cos \frac{(n-4)\theta_m}{2} \right\} \\ g_{n,m} &= \frac{-r_m^{\frac{n}{2}}}{2\mu} \left\{ \left[\kappa + \frac{n}{2} - (-1)^n \right] \sin \frac{n\theta_m}{2} - \frac{n}{2} \sin \frac{(n-4)\theta_m}{2} \right\} \\ h_{n,m} &= \frac{r_m^{\frac{n}{2}}}{2\mu} \left\{ \left[\kappa - \frac{n}{2} - (-1)^n \right] \sin \frac{n\theta_m}{2} + \frac{n}{2} \sin \frac{(n-4)\theta_m}{2} \right\} \\ l_{n,m} &= \frac{r_m^{\frac{n}{2}}}{2\mu} \left\{ \left[\kappa - \frac{n}{2} + (-1)^n \right] \cos \frac{n\theta_m}{2} + \frac{n}{2} \cos \frac{(n-4)\theta_m}{2} \right\} \end{aligned} \quad (9)$$

Eqs. 6 and 7 can be written in terms of the SIF and T-stress as follows [21]:

$$u = \frac{K_I}{2\mu} \sqrt{\frac{r}{2\pi}} \cos \frac{\theta}{2} \left(\kappa - 1 + 2 \sin^2 \frac{\theta}{2} \right) + \frac{K_{II}}{2\mu} \sqrt{\frac{r}{2\pi}} \sin \frac{\theta}{2} \left(\kappa + 1 + 2 \cos^2 \frac{\theta}{2} \right) + \frac{T}{8\mu} r (\kappa + 1) \cos \theta \quad (10)$$

$$v = \frac{K_I}{2\mu} \sqrt{\frac{r}{2\pi}} \sin \frac{\theta}{2} \left(\kappa + 1 - 2 \cos^2 \frac{\theta}{2} \right) - \frac{K_{II}}{2\mu} \sqrt{\frac{r}{2\pi}} \cos \frac{\theta}{2} \left(\kappa - 1 - 2 \cos^2 \frac{\theta}{2} \right) + \frac{T}{8\mu} r (\kappa - 3) \sin \theta \quad (11)$$

It can be shown that

$$K_I = a_1 \sqrt{2\pi}, \quad K_{II} = -b_1 \sqrt{2\pi}, \quad T = 4a_2$$

where K_I and K_{II} are the mode I and II of the SIF, respectively, and T represents T-stress. The effects of adding non-singular terms [76] (up to 10 terms) in Williams' solution was also explored.

The results were then validated by comparison with nominal SIF solution ($K_{I \text{ nom}}$) [77]. Since nominal values do not include any closure effect, care was taken to generate results with as little influence as possible from closure-related mechanisms. To this end, ΔK_I and load ratio were increased from 8 MPa. \sqrt{m} and 0.1 in the fatigue pre-cracking step to 11 MPa. \sqrt{m} and 0.3 during the cycles used for evaluating the SIF [78].

The accuracy of experimental results was then examined through the δ parameter defined as follows:

$$\delta = \left| \frac{K_{I \text{ exp}} - K_{I \text{ nom}}}{K_{I \text{ nom}}} \right| \times 100 \quad (12)$$

where $K_{I \text{ exp}}$ is evaluated with equation (1) and $K_{I \text{ nom}}$ is computed from [77]. Low δ indicates more accurate estimations of K_I .

In order to evaluate the effect of the AOI position, λ is defined as:

$$\lambda = \frac{a_{in}}{L} \times 100 \quad (13)$$

where a_{in} is the length of a part of the crack inside AOI and L represents the longitude length of the AOI.

To study the effect of the size of the AOI on the estimation of SIFs, six different AOIs in a constant FOV were analysed (Fig. 9). Minimum required data points in an AOI of $1 \times 1 \text{ mm}^2$ for an estimation error less than 10% (δ) is also examined.

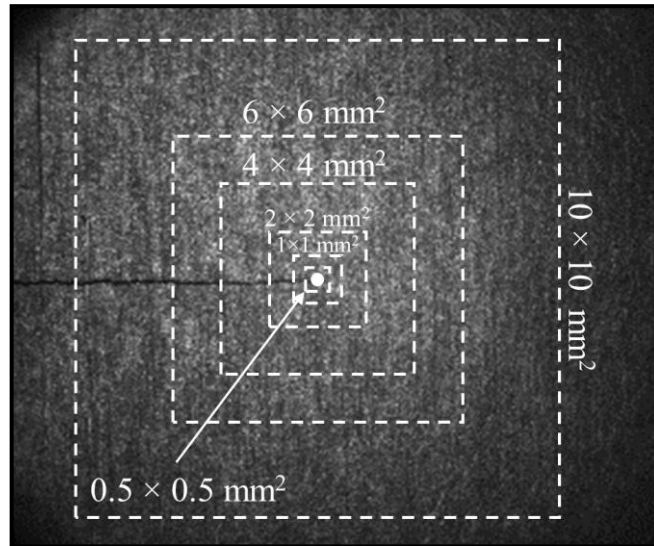


Figure 9. The difference between FOV and AOI. The FOV is the size of the whole image. Six different AOIs are defined within the FOV when $\lambda = 50\%$.

3.2. SIF monitoring by DIC

The experiment of this part is similar to the previous part, except for the loading sequences in which the cyclic loads were applied in a ramp wave form with load ratio of 0.3 with five different applied nominal ΔK_I of 10, 15, 20, 25 and 30 $\text{MPa}\sqrt{\text{m}}$. At the end of cyclic loads, the load was increased constantly until the sudden fracture of the sample occurs under load control. Fig. 10 shows the schematic of the loading sequences.

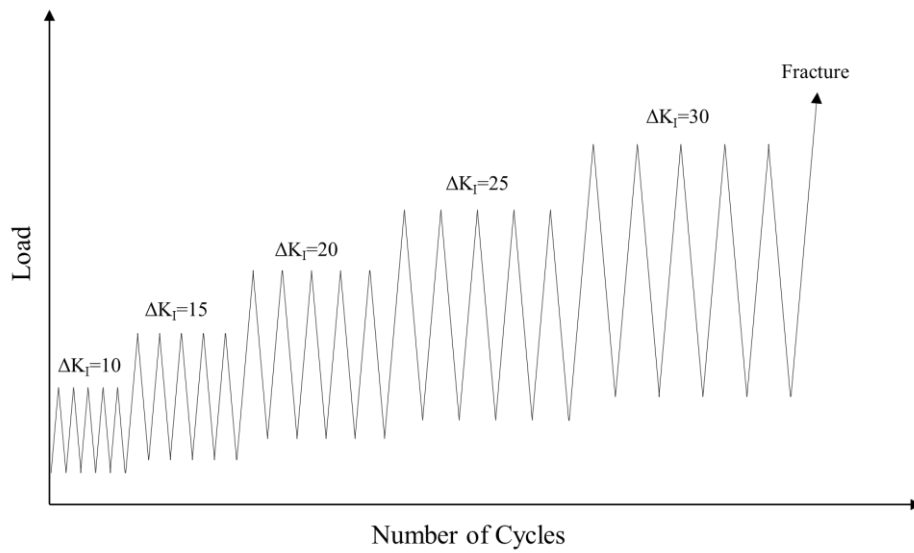


Figure 10. Schematic of loading sequences.

3.3. Biaxial experiment

In the third part of this work, crack propagation in a low carbon steel (St-52-3N) was studied by using DIC. Fig. 11 illustrates the microstructure of the material obtained by optical microscope which shows the ferrite and pearlite bands [79]. The mechanical properties of the alloy are given in Table 3. A schematic of the geometry is shown in Fig. 12.

Table 3. Monotonic properties of St-52-3N steel [79].

Yield stress, σ_y	386 MPa
Ultimate tensile stress, σ_u	639 MPa
Young's modulus, E	206 GPa
Shear Modulus	78 GPa

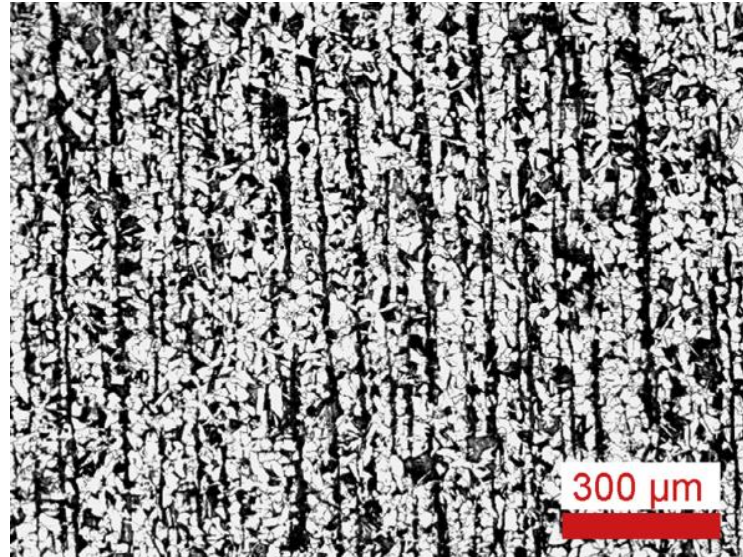


Figure 11. The microstructure of St52-3N steel. Black and white vertical bands are showing the pearlite and ferrite bands, respectively [79].

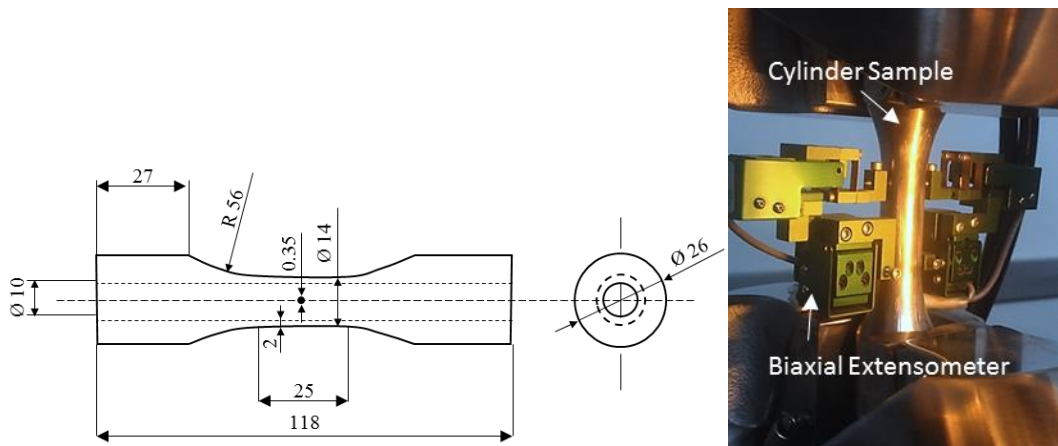


Figure 12. The geometry of the hollow cylinder specimen with a central hole. All dimensions are in mm.

An MTS 809 servo-hydraulic loading rig coupled by a biaxial extensometer Epsilon 3550 was used to apply biaxial loads under stress control mode in a similar way to previous works [80,81]. In-phase cyclic sinus signal with axial load ratio of 0.1 ($R_a = 0.1$) and torsional load ratio of -1 ($R_t = -1$) was applied in air at room temperature. A hole with a diameter of about 0.35 mm was drilled in the outer surface of the specimen in order to enforce the crack to nucleate inside the FOV (Fig. 12).

In order to study the effect of the overload (OL) on the crack propagation behaviour, single OL cycle ($\Delta\sigma_{OL}$, $\Delta\tau_{OL}$) was applied on specimens on the half of the final crack length with the axial and torsional load ratio of 0.1 and -1, respectively. Tests were performed under two different baseline loads. Single OL cycles of 40% and 100% were applied on S2 and S4 samples respectively. The overload value was defined as follows:

$$OL\% = \left(\frac{\Delta\sigma_{OL} - \Delta\sigma}{\Delta\sigma} \right) \quad (14)$$

The secant method recommended in ASTM E647-15e1 standard [73] has been employed to examine the rate of the fatigue crack growth. Table 4 shows the loading condition for samples with and without OL.

In addition, to evaluate the closure level, near tip COD was measured by DIC [62,82]. Fig 13 shows the positions of the virtual extensometer and crack initiation angle for S2 sample as an example.

Table 4. Axial and shear stress values for specimens with and without OL cycle.

Specimen	Crack length at OL (μm)	$\Delta\sigma$ (MPa)	$\Delta\tau$ (MPa)	$\Delta\sigma_{OL}$ (MPa)	$\Delta\tau_{OL}$ (MPa)
S1	-	216	277	-	-
S2	669	216	277	302.4	388
S3	-	162	230	-	-
S4	689	162	230	324	460

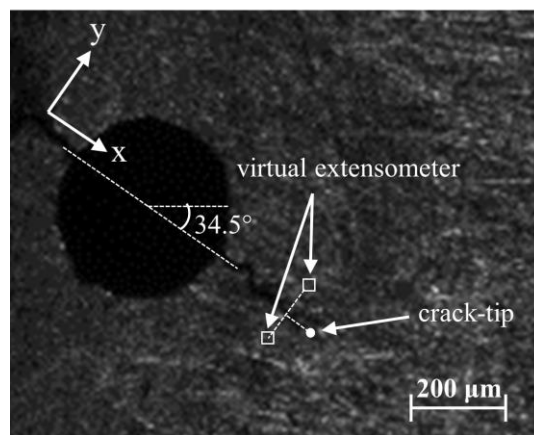


Figure 13. The position of virtual extensometers for COD examination. The white bold mark shows the crack-tip position.

The effect of single OL was studied by observing the evolution of the crack length versus the number of cycles. Fig. 14 shows how applying a single OL cycle can affect the crack growth behaviour for two different baseline loads. Fig. 14.a shows that high loads produced lives of 58000 and 66000 cycles for the specimens with no OL (S1) and with OL (S2), respectively. Fig. 14.b shows that low loads produced lives of 136000 and 138000 cycles for the specimens with no OL (S3) and with OL (S4), respectively. The crack growth rate is plotted as a function of crack length in Fig. 15. The overall higher da/dN values in Fig. 15.a than in Fig. 15.b indicate that growth rates observed in high load tests are on average 8 times faster than rates in low load tests.

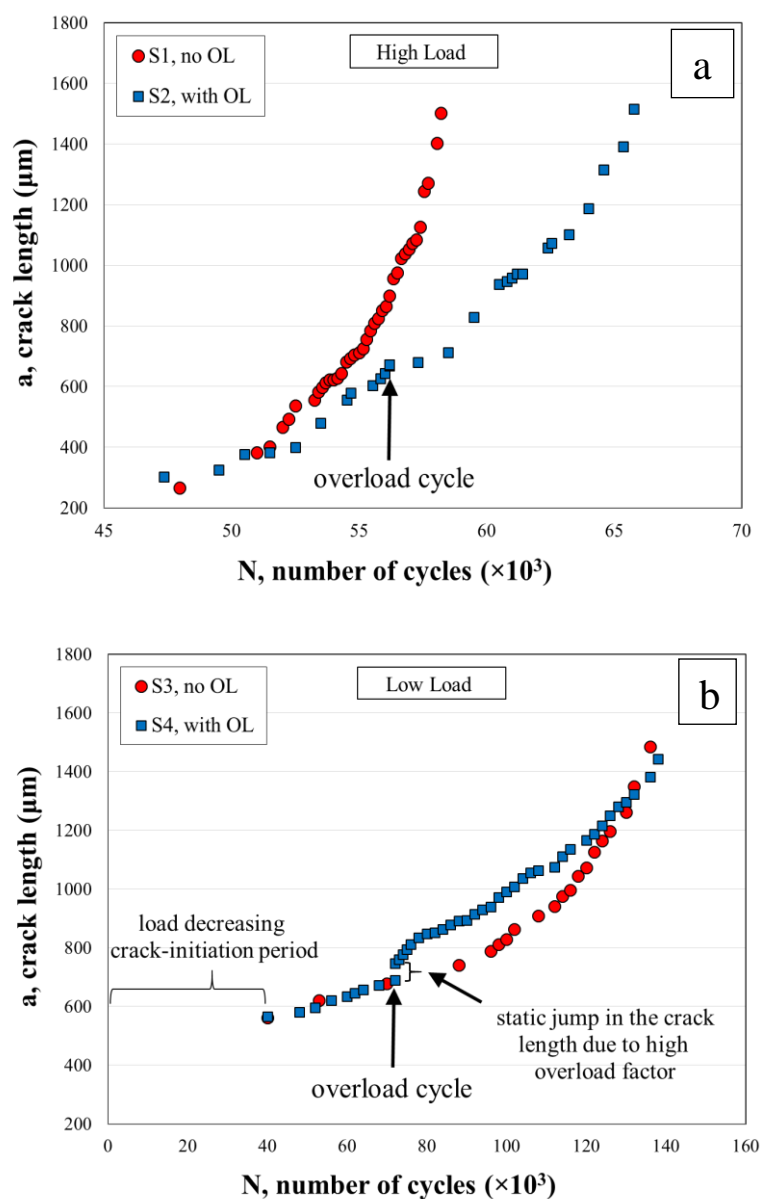


Figure 14. Evolution of crack length versus number of cycles for samples with and without OL cycle, a) samples S1 and S2 under higher cyclic loads, b) samples S3 and S4 under lower cyclic loads.

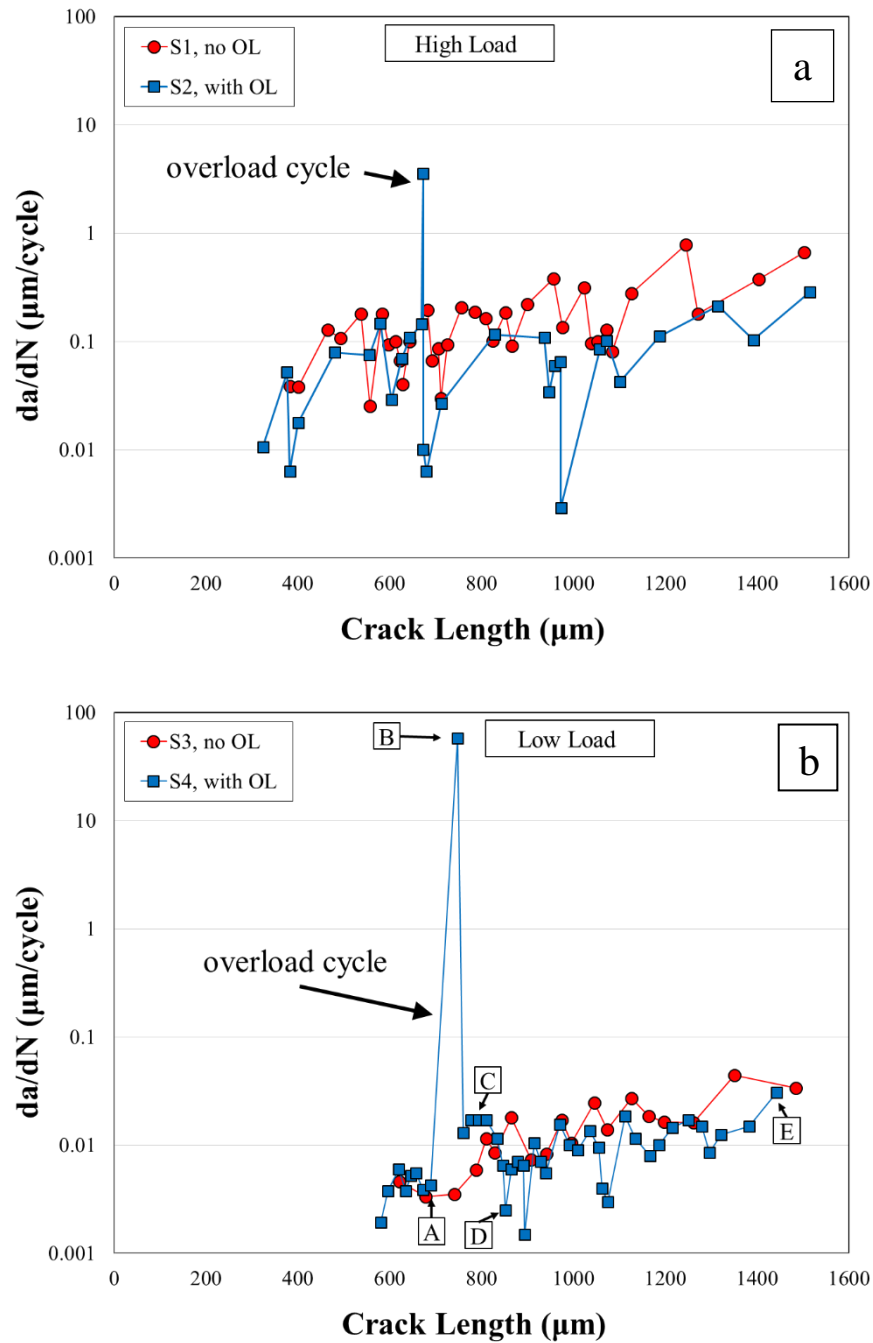


Figure 15. Crack growth rate as a function of the crack length for high (a) and low (b) baseline cyclic load.

The displacement field were extracted by DIC with the similar parameters as for previous experiment. By taking into account the size of the AOI ($0.4 \times 0.4 \text{ mm}^2$), two terms in the Williams' solution were used as suggested in [83].

In order to extract the vertical and the horizontal displacements with respect to the axial loading axis, captured images have been rotated so that the crack appears horizontal in all

images. Fig. 16 illustrates the vertical displacement contour for an AOI around a crack with a length of 0.689 mm (sample S2). The images were rotated 37° clockwise so that the crack line was horizontal [59]. Displacement data points inside an area of 0.4×0.4 mm² were extracted and fitted to Williams' solution to calculate the SIFs.

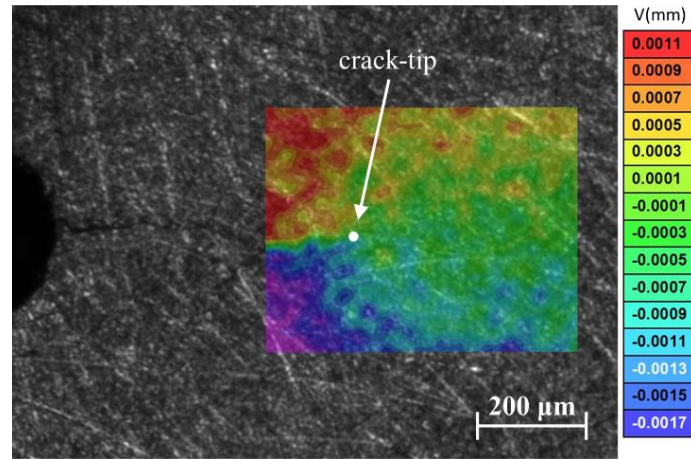


Figure 16. The position of the AOI for deriving the displacement field ahead of a crack with the length of 0.669 mm after 53500 cycles (sample S2). The image has been rotated, so that the crack line becomes horizontal.

The COD was also evaluated from the DIC data. A post processing routine was developed to measure the COD with a virtual extensometer as follows:

$$COD(x) = v_{bot} - v_{top} \quad (15)$$

where v is the vertical displacement and x is the distance of the extensometer behind the crack-tip (here $x = 60 \mu\text{m}$). The subscripts “top” and “bot” refer to the position of the virtual extensometer points relative to the crack line. The compliance based algorithm proposed by Skorupa et al. [84] has been utilised to study the fatigue crack closure in this study. This method has been used by other authors for characterising fatigue crack closure using local compliance measurements [85].

4. Results and discussion

4.1. Optimizing DIC parameters for SIF measurement

In the first part of the experiments, the experimental parameters of DIC method for evaluation of the SIF were examined. It was observed that by increasing the subset size from 13 to 200 pixels ($FOV = 6 \times 6 \text{ mm}^2$), the E (standard Deviation Confidence Interval) decreased while the error of SIF estimation (δ) increased steadily. Increasing δ as a result of enlarging the subset size is probably due to the low resolution in the displacement field in the crack-tip region, where large gradients occur.

It was also observed that omitting or considering the crack tip plastic zone in the post-processing step does not have a considerable effect on the estimation of SIF. This behaviour can be explained by noting that, unlike with stress field, there is no singularity at the crack-tip for displacement field [86].

To study the effect of the area where displacement data are collecting relative to the crack tip position, the λ parameter was introduced in section 2. The results of estimating the SIF for different λ parameters and different FOVs are summarised in Fig. 17. The curves corresponding to different FOVs show a minimum in δ for λ parameter of 25%. That is, for all FOVs, the best results are obtained when the crack-tip is included in the AOI and crack extends over one fourth of the FOV.

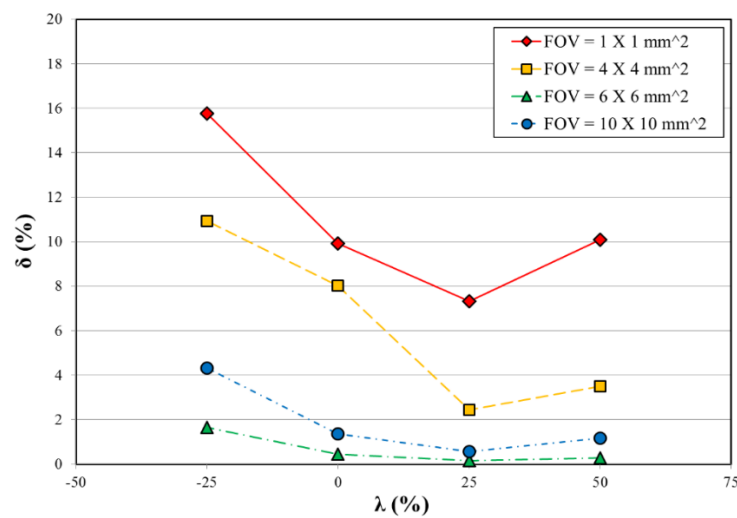


Figure 17. The behaviour of δ as a function of λ for different FOVs. Nine terms in Williams' expansion were used in all cases.

The next parameter that will be studied is the size of the FOV. It was observed that beyond FOV larger than 4 mm, more terms of Williams' expansion are required to obtain good estimations. This behaviour is logical since higher order terms are required for describing accurately large crack-tip fields.

The effect of selecting different sizes of AOI in a large FOV was also investigated and it was observed that using a small AOI (even one-tenth of the FOV) will result in the same accuracy as using small FOV by utilising high magnification lenses. One of the advantages of using small AOI is the fewer number of data points required to be analysed.

This observation suggests that the system of equations solved to evaluate the SIF is excessively and unnecessarily over-determined. The degree of over-determination in the multi-point over-deterministic method can be studied through the parameter ϕ , defined as:

$$\phi = \frac{\text{number of data points}}{\text{number of terms in series}} \quad (16)$$

Fig. 18 shows the accuracy of SIF estimation for different values of ϕ .

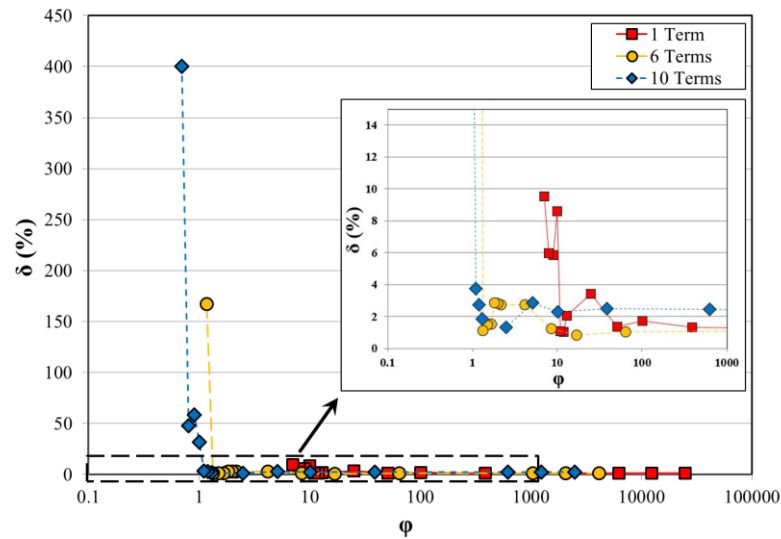


Figure 18. Effect of reducing data points in an AOI of $4 \times 4 \text{ mm}^2$ where $\lambda = 25\%$. ϕ is defined as the number of data points used in the analysis divided by the number of terms in the series. Note the logarithmic scale in ϕ scale.

It can be seen the value of δ remains stable as long as $\phi > 15$. Fig. 18 also shows that decreasing ϕ from 1.1 to 0.7 (or reducing the data points from 11 to 7) made a drastic increase in δ from 3.74% to 400% for calculations based on 10 terms. Very similar trends were also observed for other FOVs. This analysis suggests that in the optimum condition ($\lambda = 25\%$, $\text{FOV} > 4 \times 4 \text{ mm}^2$), reliable SIF estimations ($\delta < 4\%$) can be obtained as long as $\phi > 15$.

4.2. SIF monitoring by DIC

In this part of the experiment, the displacement field ahead of a fatigue crack was monitored continuously by DIC method. Five terms in Williams' expansion were used to describe the crack tip field because no further improvement in the fitting of experimental to analytical displacement data observed by considering more than five terms.

In order to evaluate the ability of the proposed method to be used for in-service applications, continuous monitoring of the SIF is studied. It was observed that by increasing the applying load amplitude, the experimental ΔK always overestimates the nominal values (ΔK_{nom}). The difference becomes more significant for higher loads. This behaviour can be attributed to the development of the plastically deformed zone at the crack tip. To compensate the effect of plasticity at the nominally evaluated SIF, Irwin's approach [87] was used. To this end, the crack tip was located at the centre of the plastic zone. In other words, the crack length was computed as the sum of crack length (a) with the half of the plastic zone (r_y):

$$a_{\text{corr}} = a + r_y \quad (17)$$

where

$$r_y = \frac{1}{2\pi} \left(\frac{K_I}{\sigma_{ys}} \right)^2 \quad (18)$$

Accordingly, the nominal SIF was recalculated by replacing the crack length with the corrected crack length (a_{corr}) [88,89]. Fig. 19 shows how crack length correction can significantly improve the accuracy of the nominal SIF evaluation for higher loads, while it has a negligible effect at low ΔK . For example, for $\Delta K = 30 \text{ MPa}\sqrt{\text{m}}$ the value of δ is reduced by 24.6%, 23.6% and 23.2% for AOIs of 10×10 , 15×15 and $20 \times 20 \text{ mm}^2$, respectively. The plasticity correction has reduced the value of δ at $\text{AOI} = 20 \times 20 \text{ mm}^2$ by 7.9%, 14.9% and

23.2% for applied ΔK of 20, 25 and 30 $\text{MPa}\sqrt{\text{m}}$, respectively. The higher value of δ at $\Delta K=10$ $\text{MPa}\sqrt{\text{m}}$ rather $\Delta K=15$ $\text{MPa}\sqrt{\text{m}}$ can be attributed to the poorer noise to signal ratio at lower applied loads.

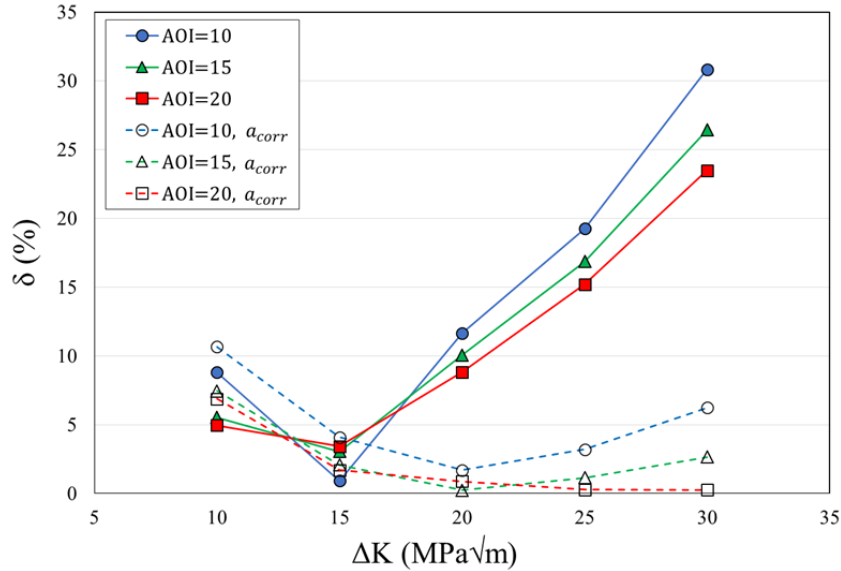


Figure 19. Evolution of δ by increasing ΔK_{nom} for different sizes of AOI in mm.

Fig. 20 shows the evolution of SIFs as a function of the applied load during the last loading segment, leading to the fracture of the sample. It can be observed that by increasing the load, the difference between the experimental and nominal SIF becomes more significant. The graph in Fig. 20 shows a very good fit between ΔK_{exp} and ΔK_{corr} up to the $\Delta K \approx 42$ $\text{MPa}\sqrt{\text{m}}$ where there is a linear relation between SIF and load range (ΔP). Thereafter, ΔK_{exp} surges upward while ΔK_{nom} keeps increasing linearly. Sudden fracture happened just after the last measurement point (top-right photograph in Fig. 20). Considering the load ratio of 0.3, at the deviation point, the K_{max} is about 55 $\text{MPa}\sqrt{\text{m}}$ ($\Delta K \approx 42$ $\text{MPa}\sqrt{\text{m}}$). It is interesting that this value is in good agreement with the estimated K_c by Newman et al. [90] for a sample with similar geometry and thickness. This suggests that the point at which ΔK deviates from the linear behaviour can be used to estimate the critical SIF for this thickness. The higher value for measured critical SIF rather the fracture toughness of this material can be attributed to thinner thickness of the sample than standard samples for fracture toughness test [91].

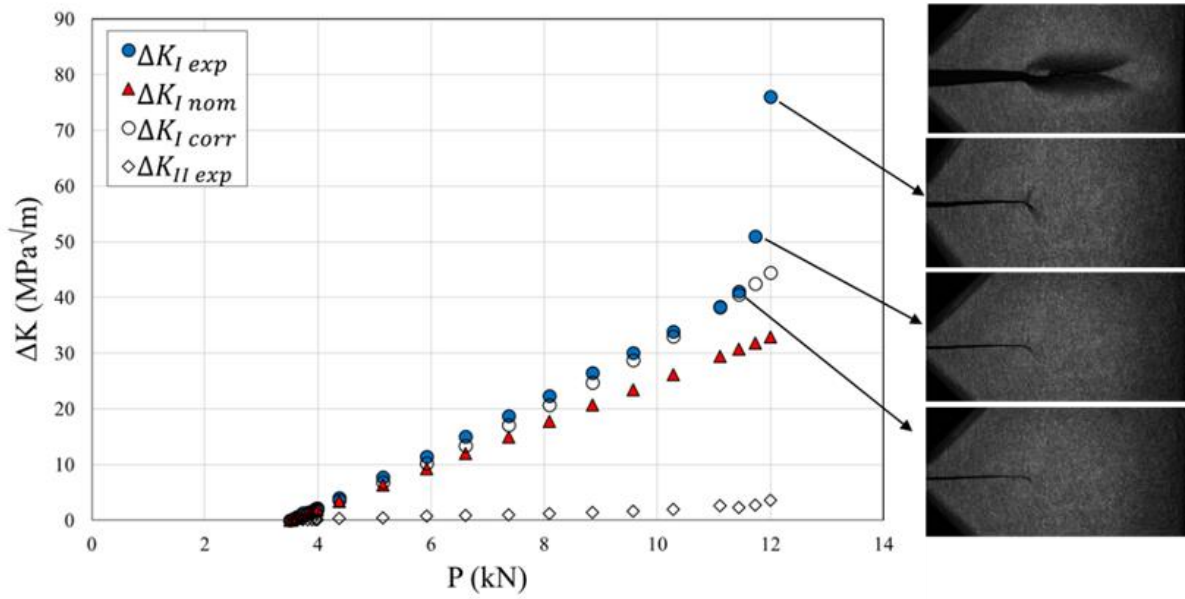


Figure 20. Continuous evaluation of ΔK as a function of applied load at the last loading segment, leading to sudden fracture of the sample.

4.3. Biaxial experiment

The capability of the proposed hybrid method for studying the crack state under complex loading condition was evaluated by studying a crack under tension-torsion cyclic loads which experienced an OL cycle.

The evolution of COD during a complete cycle (loading and unloading) at 60 μm behind the crack-tip for different crack lengths in all samples is shown in Fig. 21. For the specimens not subjected to OL, the maximum COD in a cycle increases steadily with the crack length (Figs. 21.a and c). There is a more drastic increment as the crack grows in the COD for high baseline load (Fig. 21.a) than for the low baseline load (Fig. 21.c), as one would expect.

The effect of applying an OL cycle on COD behaviour of samples can be seen in Fig. 21b and d. It can be seen that 40% OL in sample S2, produced a reduction in the maximum COD by the end of the test of 64% while 100 % OL cycle in sample S4 produced only 38% reduction in COD.

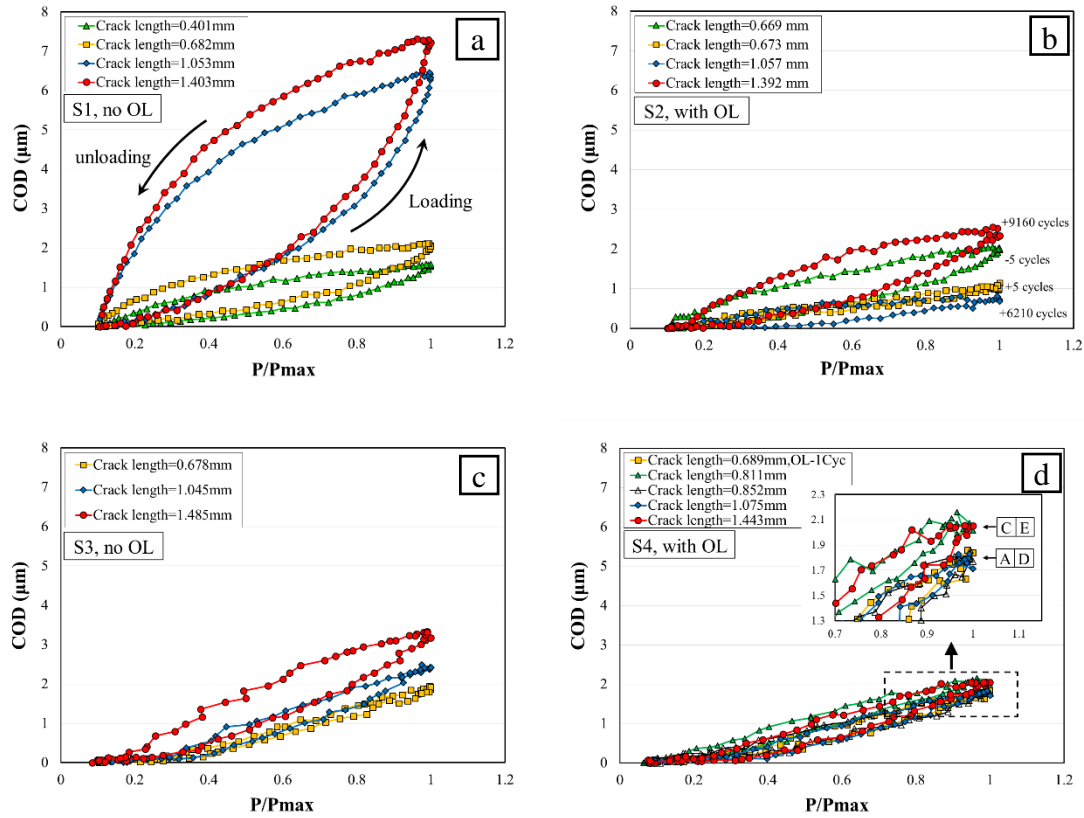


Figure 21. COD behaviour during loading and unloading cycle for different crack lengths of specimens. The number of cycles before and after OL where OL cycle was considered as 0 cycles, are shown in the graph b.

A summary of the opening load estimated following the procedure described in previous section is shown in Table 5. It can be seen that P_{op} for S1 is 19% of the P_{max} , whereas P_{op} for S2 sample, which has experienced an OL cycle, is 27% of the P_{max} . Regarding samples S3 and S4 which were tested under a lower baseline load, the OL cycle only increased P_{op} slightly at the longest crack length. The P_{op} increment induced by the OL is larger for low loads than for high loads (Table 5). This agrees well with the change that the OL produces in the growth rate (Fig. 14). The difference between the OL and the non-OL curves in crack growth rate is larger for low loads (Fig. 15.a) than for high loads (Fig. 15.b). Thus, crack growth rate data correlate satisfactorily with opening loads.

Table 6 shows the evaluated SIFs and corresponding COD_{max} for two different crack lengths on each sample. It can be seen that ΔK_I and ΔK_{II} increase as the crack grows from 0.682 mm to 1.053 mm for sample S1 and from 0.675 mm to 1.045 mm for sample S3. Figs. 21.b and 21.d show that applying an OL reduces the COD values, as long as the crack is within the retardation stage. The small differences in the trend of ΔK_I and ΔK_{II} values are probably due

to the crack changing its orientation through the experiment [79] as a consequence of crack-tip plasticity [92,93], loading direction and microstructure.

Table 5. Crack opening loads in a complete cycle

Sample	P_{op}/P_{max}
S1	0.19
S2	0.27
S3	0.29
S4	0.31

Table 6. Summary of the SIFs estimated for different samples and different crack lengths

Specimen	Crack length (mm)	COD_{max} (μm)	ΔK_I ($MPa\sqrt{m}$)	ΔK_{II} ($MPa\sqrt{m}$)
S1	0.682	2.1	13.2	24.5
	1.053	6.3	36.8	40.0
S2	0.669	2.0	13.1	20.4
	1.057	0.7	15.6	25.3
S3	0.678	1.9	11.8	0.2
	1.045	2.4	19.7	0.3
S4	0.689	1.9	11.9	1.6
	1.075	1.8	14.0	3.7

5. Conclusions

In this work, the efficacy of a proposed hybrid method for evaluation of SIF was examined by performing different experiments. The proposed method is based on multi-parameter fracture mechanics where full-field experimental displacement data are captured. The experimental information is measured in the region surrounding the tip of a fatigue crack and then fitted to an analytical displacement field (Williams' series). Finally, the SIFs were estimated using a multipoint over deterministic method. In the first experiment, the effect of some experimental variables on K_I estimation using DIC was examined based on an elastic mode I. It was shown that the accuracy of K_I can be affected not only by the well-known variables such as subset size in DIC and considered number of Williams' series but also by the size and position of AOI. Experimental results indicate the significant effect of the position of the AOI for accurate estimation of SIF with DIC technique. It was shown that including a part of the crack length inside the AOI (crack extending to one-fourth of the AOI) provides the best estimations for all FOVs. Finally, it was also shown that reliable estimations of the K_I can be achieved as long as the number of displacement vectors fitted to the model is 15 times larger than the number of terms in the series.

In a similar manner, the evolution of SIF was monitored by DIC method in a separate experiment. The results showed that the Irwin's approach that modifies the crack length to account for crack tip plasticity improves noticeably the SIF estimations. Continuous measurement of the SIF at the final loading stage to fracture of the sample showed a deviation from the linear relation between the load and the experimental SIF. Based on a previous work, this deviation might be related to the critical SIF for the thickness studied. Since either the experimental method or corrected theoretical method are based on LEFM, the validity of the results in this range should be assessed with a parameter like J-integral. Nevertheless, further research is currently in progress to better understand the physics behind such deviation.

The capability of the proposed method for capturing the SIF of a crack under more complex loading condition was also assessed. In addition, the effect of applying OL cycle on the behaviour of a crack under cyclic biaxial loading is studied with DIC technique. It is observed that applying 100% OL on a sample under low cyclic loads, delayed the appearance of the retardation stage. COD examinations shows the classical sequences of OL, including acceleration and retardation. The hybrid method was also used for studying the biaxial fatigue

cracks. This allowed the mixed-mode SIF (ΔK_I and ΔK_{II}) to be estimated on samples under different load levels, with and without applying OL. Results showed that a slower increment in ΔK_I as the crack grows for the OL case, compared to the non-OL case.

The results of three experiments proved the reliability and capability of the hybrid method for evaluation of SIFs not only for simple uniaxial conditions, but also for more complex biaxial loading conditions. The suggested recommendations for selecting the experimental DIC parameters can be used by researchers and engineers for improving the accuracy and stability of SIF measurement using DIC technique. The SIF monitoring experiment showed the capability of the method for in-service application, when evolution of the SIF needs to be measured continuously.

References

- [1] T.L. Anderson, *Fracture Mechanics, Fundamentals and Applications*, 4th ed., CRC Press, Boca Raton, FL, USA., 2017.
- [2] S. Suresh, *Fatigue of Materials*, 2nd ed., Cambridge University Press, New York, 1998.
- [3] K. Ramesh, S. Gupta, A.A. Kelkar, Evaluation of stress field parameters in fracture mechanics by photoelasticity - revisited, *Eng. Fract. Mech.* 56 (1997) 25-41 and 43-45.
- [4] F.A. Díaz, J.R. Yates, E.A. Patterson, Some improvements in the analysis of fatigue cracks using thermoelasticity, *Int. J. Fatigue.* 26 (2004) 365–376. doi:10.1016/j.ijfatigue.2003.08.018.
- [5] D. Nowell, R.J.H. Paynter, P.F.P. De Matos, Optical methods for measurement of fatigue crack closure: moiré interferometry and digital image correlation, *Fatigue Fract. Eng. Mater. Struct.* 33 (2010) 778–790. doi:10.1111/j.1460-2695.2010.01447.x.
- [6] S.R. McNeill, W.H. Peters, M.A. Sutton, Estimation of stress intensity factor by digital image correlation, *Eng. Fract. Mech.* 28 (1987) 101–112. doi:10.1016/0013-7944(87)90124-X.
- [7] J. Smith, M.N. Bassim, C.D. Liu, T.M. Holden, Measurement of crack tip strains using neutron diffraction, *Eng. Fract. Mech.* 52 (1995) 843–851.
- [8] P. Lopez-Crespo, P.J. Withers, F. Yusof, H. Dai, a. Steuwer, J.F. Kelleher, T. Buslaps, Overload effects on fatigue crack-tip fields under plane stress conditions: surface and bulk analysis, *Fatigue Fract. Eng. Mater. Struct.* 36 (2013) 75–84. doi:10.1111/j.1460-2695.2012.01670.x.
- [9] S. Yoneyama, A. Kitagawa, S. Iwata, K. Tani, H. Kikuta, Bridge deflection measurement using digital image correlation, *Exp. Tech.* 31 (2007) 34–40. doi:10.1111/j.1747-1567.2007.00132.x.
- [10] M.A. Sutton, N. Li, D.C. Joy, A.P. Reynolds, X. Li, Scanning electron microscopy for quantitative small and large deformation measurements Part I: SEM imaging at magnifications from 200 to 10,000, *Exp. Mech.* 47 (2007) 775–787. doi:10.1007/s11340-007-9042-z.
- [11] J.D. Carroll, W. Abuzaid, J. Lambros, H. Sehitoglu, High resolution digital image

- correlation measurements of strain accumulation in fatigue crack growth, *Int. J. Fatigue*. 57 (2013) 140–150. doi:10.1016/j.ijfatigue.2012.06.010.
- [12] R. Stephens, A. Fatemi, R.R. Stephens, H. Fuchs, *Metal Fatigue in Engineering*, 2nd ed., John Wiley & Sons, Inc, New York, 2001.
 - [13] ASTM E1823-13 Standard Terminology Relating to Fatigue and Fracture Testing, West Conshohocken, PA, 2013. doi:10.1520/E1823-13.2.
 - [14] G.R. Irwin, Analysis of stresses and strains near the end of a crack traversing a plate, *J. Appl. Mech. ASME*. E24 (1957) 351–369.
 - [15] P.P. Paris, F.F. Erdogan, A critical analysis of crack propagation laws, *ASME. J. Basic Eng.* 85 (1963) 528–533. doi:doi:10.1115/1.3656900.
 - [16] M.A. Sutton, J.-J. Orteu, H.W. Schreier, *Image Correlation for Shape, Motion and Deformation Measurements*, Springer US, New York, 2009. doi:10.1007/978-0-387-78747-3.
 - [17] P.F.P. de Matos, D. Nowell, Numerical simulation of plasticity-induced fatigue crack closure with emphasis on the crack growth scheme: 2D and 3D analyses, *Eng. Fract. Mech.* 75 (2008) 2087–2114. doi:10.1016/j.engfracmech.2007.10.017.
 - [18] H.M. Westergaard, Bearing pressures and cracks, *J. Appl. Mech.* 61 (1939) A49–A53.
 - [19] M.L. Williams, On the stress distribution at the base of a stationary crack, *J. Appl. Mech.* 24 (1957) 109–114. doi:10.1115/1.3640470.
 - [20] B.S.G. Larsson, A.J. Carlsson, Influence of non-singular stress terms and specimen geometry on small-scale yielding at crack tips in elastic-plastic materials, *J. Mech. Phys. Solids*. 21 (1973) 263–277.
 - [21] J.R. Yates, M. Zanganeh, Y.H. Tai, Quantifying crack tip displacement fields with DIC, *Eng. Fract. Mech.* 77 (2010) 2063–2076. doi:10.1016/j.engfracmech.2010.03.025.
 - [22] C.J. Christopher, M.N. James, E.A. Patterson, K.F. Tee, Towards a new model of crack tip stress fields, *Int J Fract.* 148 (2007) 361–371. doi:10.1007/s10704-008-9209-3.
 - [23] P. Lopez-Crespo, D. Camas, F.V. Antunes, J.R. Yates, A study of the evolution of crack tip plasticity along a crack front, *Theor. Appl. Fract. Mech.* 98 (2018) 59–66. doi:10.1016/J.TAFMEC.2018.09.012.
 - [24] R.O. Ritchie, Mechanisms of fatigue crack propagation in metals, ceramics and

- composites: Role of crack tip shielding, *Mater. Sci. Eng. A.* 103 (1988) 15–28. doi:10.1016/0025-5416(88)90547-2.
- [25] M.A. Sutton, W. Zhao, S.R. McNeill, J.D. Helm, R.S. Piascik, W.T. Riddell, Local crack closure measurements: development of a measurement system using computer vision and a far-field microscope, in: R.C. McClung, J.C. Newman (Eds.), *Adv. Fatigue Crack Clos. Meas. Anal. Second Vol. ASTM STP 1343*, American Society for Testing and Materials, West Conshohocken, PA, 1999: pp. 145–156.
- [26] C.A. Simpson, S. Kozuki, P. Lopez-Crespo, M. Mostafavi, T. Connolley, P.J. Withers, Quantifying fatigue overload retardation mechanisms by energy dispersive X-ray diffraction, *J. Mech. Phys. Solids.* 124 (2019) 392–410. doi:10.1016/J.JMPS.2018.10.020.
- [27] A.S. Chernyatin, P. Lopez-Crespo, B. Moreno, Y.G. Matvienko, Multi-approach study of crack-tip mechanics on aluminium 2024 alloy, *Theor. Appl. Fract. Mech.* 98 (2018) 38–47. doi:10.1016/J.TAFMEC.2018.09.007.
- [28] S. Stoychev, D. Kujawski, Methods for crack opening load and crack tip shielding determination: A review, *Fatigue Fract. Eng. Mater. Struct.* 26 (2003) 1053–1067. doi:10.1046/j.1460-2695.2003.00691.x.
- [29] M.A. Sutton, W.J. Wolters, W.H. Peters, W.F. Ranson, S.R. McNeill, Determination of displacements using an improved digital correlation method, *Image Vis. Comput.* 1 (1983) 133–139. doi:10.1016/0262-8856(83)90064-1.
- [30] M.R. Ayatollahi, H. Safari, Evaluation of crack tip constraint using photoelasticity, *Int. J. Press. Vessel. Pip.* 80 (2003) 665–670. doi:10.1016/S0308-0161(03)00076-0.
- [31] S. Yoneyama, T. Ogawa, Y. Kobayashi, Evaluating mixed-mode stress intensity factors from full-field displacement fields obtained by optical methods, *Eng. Fract. Mech.* 74 (2007) 1399–1412. doi:10.1016/j.engfracmech.2006.08.004.
- [32] B. Pan, K. Qian, H. Xie, A. Asundi, Two-dimensional digital image correlation for in-plane displacement and strain measurement: a review, *Meas. Sci. Technol.* 20 (2009) 062001 (17pp). doi:10.1088/0957-0233/20/6/062001.
- [33] J.R. Taylor, *An introduction to error analysis: the study of uncertainties in physical measurements*, 2nd ed., California, 1982. doi:10.1119/1.13309.
- [34] H.W. Schreier, J.R. Braasch, M.A. Sutton, Systematic errors in digital image correlation

- caused by intensity interpolation, *Opt. Eng.* 39 (2000) 2915–2921.
- [35] H.W. Schreier, M.A. Sutton, Systematic errors in digital image correlation due to undermatched subset shape functions, *Exp. Mech.* 42 (2002) 303–310. doi:10.1177/001448502321548391.
 - [36] L. Yu, B. Pan, The errors in digital image correlation due to overmatched shape functions, *Meas. Sci. Technol.* 26 (2015) 045202. doi:10.1088/0957-0233/26/4/045202.
 - [37] M. Fazzini, S. Mistou, O. Dalverny, L. Robert, Study of image characteristics on digital image correlation error assessment, *Opt. Lasers Eng.* 48 (2010) 335–339. doi:10.1016/j.optlaseng.2009.10.012.
 - [38] B. Pan, Reliability-guided digital image correlation for image deformation measurement, *Appl. Opt.* 48 (2009) 1535–1542. doi:10.1364/AO.48.001535.
 - [39] J.M. Vasco-Olmo, F.A. Díaz, E.A. Patterson, Experimental evaluation of shielding effect on growing fatigue cracks under overloads using ESPI, *Int. J. Fatigue*. 83 (2016) 117–126. doi:10.1016/j.ijfatigue.2015.10.003.
 - [40] F. Berto, P. Lazzarin, On higher order terms in the crack tip stress field, *Int. J. Fract.* 161 (2010) 221–226. doi:10.1007/s10704-010-9443-3.
 - [41] F. Berto, P. Lazzarin, Multiparametric full-field representations of the in-plane stress fields ahead of cracked components under mixed mode loading, *Int. J. Fatigue*. 46 (2013) 16–26. doi:10.1016/j.ijfatigue.2011.12.004.
 - [42] M.Y. Dehnavi, S. Khaleghian, A. Emami, M. Tehrani, N. Soltani, Utilizing digital image correlation to determine stress intensity factors, *Polym. Test.* 37 (2014) 28–35. doi:10.1016/j.polymertesting.2014.04.005.
 - [43] W.H. Peters, W.F. Ranson, J.F. Kalthoff, S.R. Winkler, A study of dynamic near-crack-tip fracture parameters by digital image analysis, *J. Phys. Colloq.* 46 (1985) C5-631-C5-638. doi:10.1051/jphyscol:1985581.
 - [44] R. Hamam, F. Hild, S. Roux, Stress intensity factor gauging by digital image correlation: Application in cyclic fatigue, *Strain*. 43 (2007) 181–192. doi:10.1111/j.1475-1305.2007.00345.x.
 - [45] S. Roux, J. Réthoré, F. Hild, Recent progress in digital image correlation: from measurement to mechanical identification, *J. Phys. Conf. Ser.* 135 (2008) 012002.

doi:10.1088/1742-6596/135/1/012002.

- [46] F. Yusof, P.J. Withers, Real-time acquisition of fatigue crack images for monitoring crack-tip stress intensity variations within fatigue cycles, *J. Strain Anal. Eng. Des.* 44 (2008) 149–158. doi:10.1243/03093247JSA440.
- [47] P. Lopez-Crespo, A. Shterenlikht, J.R. Yates, E.A. Patterson, P.J. Withers, Some experimental observations on crack closure and crack-tip plasticity, *Fatigue Fract. Eng. Mater. Struct.* 32 (2009) 418–429. doi:10.1111/j.1460-2695.2009.01345.x.
- [48] D. Wagner, N. Ranc, C. Bathias, P.C. Paris, Fatigue crack initiation detection by an infrared thermography method, *Fatigue Fract. Eng. Mater. Struct.* 33 (2009) 12–21. doi:10.1111/j.1460-2695.2009.01410.x.
- [49] A. Maslouhi, Fatigue crack growth monitoring in aluminum using acoustic emission and acousto-ultrasonic methods, *Struct. Control Heal. Monit.* 18 (2011) 790–806. doi:10.1002/stc.478.
- [50] V. Zilberstein, D. Grundy, V. Weiss, N. Goldfine, E. Abramovici, J. Newman, T. Yentzer, Early detection and monitoring of fatigue in high strength steels with MWM-Arrays, *Int. J. Fatigue*. 27 (2005) 1644–1652. doi:10.1016/j.ijfatigue.2005.07.028.
- [51] R. Hamia, C. Cordier, C. Dolabdjian, Eddy-current non-destructive testing system for the determination of crack orientation, *NDT&E Int.* 61 (2014) 24–28. doi:10.1016/j.ndteint.2013.09.005.
- [52] H. Nakazawa, K. Hirano, Ultrasonic monitoring techniques of crack growth and fracture mechanics evaluation of materials, *Jpn. J. Appl. Phys.* 23 (1984) 12–16.
- [53] ASTM E1685-13, Standard practice for measuring the change in length of fasteners using the ultrasonic pulse-echo technique, in: ASTM International, West Conshohocken, PA, 2013. doi:https://doi.org/10.1520/E1685.
- [54] J. Cuadra, P.A. Vanniamparambil, K. Hazeli, I. Bartoli, A. Kontsos, A hybrid optico-acoustic NDE approach for deformation and damage monitoring, in: J. Kag, D. Jablonski, D. Dudzinski (Eds.), *Eval. Exist. New Sens. Technol. Fatigue, Fract. Mech. Testing*, STP 1584, ASTM International, West Conshohocken, PA, 2015: pp. 135–146. doi:10.1520/STP158420140051.
- [55] V.N. Whittaker, A review of non-destructive measurement of flaw size, *Non-Destructive Test.* 5 (1972) 92–100. doi:10.1016/0029-1021(72)90101-6.

- [56] P. Gao, C. Wang, Y. Li, Z. Cong, Electromagnetic and eddy current NDT in weld inspection: A review, *Insight Non-Destructive Test. Cond. Monit.* 43 (2015) 337–345. doi:10.1784/insi.2015.57.6.337.
- [57] C.B. Scruby, An introduction to acoustic emission, *J. Phys. E.* 20 (1987) 946–953. doi:10.1088/0022-3735/20/8/001.
- [58] Y. Du, F. Díaz, R. Burguete, E.A. Patterson, Evaluation using digital image correlation of stress intensity factors in an aerospace panel, *Exp. Mech.* 51 (2011) 45–57. doi:10.1007/s11340-010-9335-5.
- [59] P. Lopez-Crespo, A. Shterenlikht, E.A. Patterson, J.R. Yates, P.J. Withers, The stress intensity of mixed mode cracks determined by digital image correlation, *J. Strain Anal. Eng. Des.* 43 (2008) 769–780. doi:10.1243/03093247JSA419.
- [60] M. Zanganeh, P. Lopez-Crespo, Y.H. Tai, J.R. Yates, Locating the crack tip using displacement field data: a comparative study, *Strain.* 49 (2013) 102–115. doi:10.1111/str.12017.
- [61] S. Yoneyama, S. Arikawa, S. Kusayanagi, K. Hazumi, Evaluating J-integral from displacement fields measured by digital image correlation, *Strain.* 50 (2014) 147–160. doi:10.1111/str.12074.
- [62] P.F.P. de Matos, D. Nowell, Experimental and numerical investigation of thickness effects in plasticity-induced fatigue crack closure, *Int. J. Fatigue.* 31 (2009) 1795–1804. doi:10.1016/j.ijfatigue.2008.12.003.
- [63] D. Camas, P. Lopez-Crespo, A. Gonzalez-Herrera, B. Moreno, Numerical and experimental study of the plastic zone in cracked specimens, *Eng. Fract. Mech.* (2017). doi:10.1016/j.engfracmech.2017.02.016.
- [64] F. V. Díaz, G.H. Kaufmann, A.F. Armas, G.E. Galizzi, Optical measurement of the plastic zone size in a notched metal specimen subjected to low-cycle fatigue, *Opt. Lasers Eng.* 35 (2001) 325–333. doi:10.1016/S0143-8166(01)00030-6.
- [65] J.M. Vasco-Olmo, M.N. James, C.J. Christopher, E.A. Patterson, F.A. Díaz, Assessment of crack tip plastic zone size and shape and its influence on crack tip shielding, *Fatigue Fract. Eng. Mater. Struct.* 39 (2016) 969–981. doi:10.1111/ffe.12436.
- [66] M. Mokhtarishirazabad, P. Lopez-Crespo, M. Zanganeh, Stress intensity factor monitoring under cyclic loading by digital image correlation, *Fatigue Fract. Eng. Mater.*

- Struct. (2018). doi:10.1111/ffe.12825.
- [67] R.J. Sanford, J.W. Dally, A general method for determining mixed-mode stress intensity factors from isochromatic fringe patterns, *Eng. Fract. Mech.* 11 (1979) 621–633. doi:10.1016/0013-7944(79)90123-1.
 - [68] J. Réthoré, a. Gravouil, F. Morestin, a. Combescure, Estimation of mixed-mode stress intensity factors using digital image correlation and an interaction integral, *Int. J. Fract.* 132 (2005) 65–79. doi:10.1007/s10704-004-8141-4.
 - [69] P. López-Crespo, R.L. Burguete, E.A. Patterson, A. Shterenlikht, P.J. Withers, J.R. Yates, Study of a crack at a fastener hole by digital image correlation, *Exp. Mech.* 49 (2009) 551–559. doi:10.1007/s11340-008-9161-1.
 - [70] M. Sander, H. Richard, Experimental and numerical investigations on the influence of the loading direction on the fatigue crack growth, *Int. J. Fatigue.* 28 (2006) 583–591. doi:10.1016/j.ijfatigue.2005.05.012.
 - [71] P. Lopez-Crespo, M. Mostafavi, A. Steuwer, J.F. Kelleher, T. Buslaps, P.J. Withers, Characterisation of overloads in fatigue by 2D strain mapping at the surface and in the bulk, *Fatigue Fract. Eng. Mater. Struct.* 39 (2016) 1040–1048. doi:10.1111/ffe.12463.
 - [72] M. Mokhtarishirazabad, P. Lopez-Crespo, B. Moreno, A. Lopez-Moreno, M. Zanganeh, Optical and analytical investigation of overloads in biaxial fatigue cracks, *Int. J. Fatigue.* 100 (2017) 583–590. doi:10.1016/j.ijfatigue.2016.12.035.
 - [73] ASTM E647-15e1 Standard Test Method for Measurement of Fatigue Crack Growth Rates, ASTM International, West Conshohocken, PA, 2015. doi:10.1520/E0647-15E01.2.
 - [74] B. Moreno, An experimental analysis of fatigue crack growth under random loading, *Int. J. Fatigue.* 25 (2003) 597–608. doi:10.1016/S0142-1123(03)00018-5.
 - [75] Vic-2D software. Correlated Solutions Incorporated (C.S.Inc) <<http://www.correlatedsolutions.com>>, (n.d.).
 - [76] S. Seitzl, L. Malíková, V. Růžička, B. Moreno, P. Lopez-Crespo, Williams' expansion-based approximation of the displacement field in an Al 2024 compact tension specimen reconstructed from optical measurements, *Fatigue Fract. Eng. Mater. Struct.* 41 (2018) 2187–2196. doi:10.1111/ffe.12842.

- [77] Y. Murakami, *Stress Intensity Factors Handbook*, Oxford: Pergamon Press, 1987.
- [78] S. Beretta, S. Rabbolini, A.D. Bello, Multi-scale crack closure measurement with digital image correlation on Haynes 230, *Frat. Ed Integrità Strutt.* 33 (2015) 174–182. doi:10.3221/IGF-ESIS.33.22.
- [79] P. Lopez-Crespo, B. Moreno, A. Lopez-Moreno, J. Zapatero, Study of crack orientation and fatigue life prediction in biaxial fatigue with critical plane models, *Eng. Fract. Mech.* 136 (2015) 115–130. doi:10.1016/j.engfracmech.2015.01.020.
- [80] P. Lopez-Crespo, A. Garcia-Gonzalez, B. Moreno, A. Lopez-Moreno, J. Zapatero, Some observations on short fatigue cracks under biaxial fatigue, *Theor. Appl. Fract. Mech.* 80 (2015) 96–103. doi:10.1016/j.tafmec.2015.05.004.
- [81] P. Lopez-Crespo, B. Moreno, A. Lopez-Moreno, J. Zapatero, Characterisation of crack-tip fields in biaxial fatigue based on high-magnification image correlation and electro-spray technique, *Int. J. Fatigue.* 71 (2015) 17–25. doi:10.1016/j.ijfatigue.2014.02.016.
- [82] F. Yusof, P. Lopez-Crespo, P.J. Withers, Effect of overload on crack closure in thick and thin specimens via digital image correlation, *Int. J. Fatigue.* 56 (2013) 17–24. doi:10.1016/j.ijfatigue.2013.07.002.
- [83] M. Mokhtarishirazabad, P. Lopez-Crespo, B. Moreno, A. Lopez-Moreno, M. Zanganeh, Evaluation of crack-tip fields from DIC data: A parametric study, *Int. J. Fatigue.* 89 (2016) 11–19. doi:10.1016/j.ijfatigue.2016.03.006.
- [84] M. Skorupa, S. Beretta, M. Carboni, T. Machniewicz, An algorithm for evaluating crack closure from local compliance measurements, *Fatigue Fract. Eng. Mater. Struct.* 25 (2002) 261–273. doi:10.1046/j.1460-2695.2002.00444.x.
- [85] J.M. Vasco-Olmo, F.A. Díaz, Experimental evaluation of the effect of overloads on fatigue crack growth by analysing crack tip displacement fields, *Eng. Fract. Mech.* 166 (2016) 82–96. doi:10.1016/j.engfracmech.2016.08.026.
- [86] H.L. Ewalds, R.J.H. Wanhill, *Fracture Mechanics*, Arnold, London, 1984.
- [87] G.R. Irwin, Plastic zone near a crack and fracture toughness, in: *Sagamore Ordnance Mater. Conf.*, Syracuse University, 1961.
- [88] R.H. Heyer, D.E. McCabe, Crack growth resistance in plane-stress fracture testing, *Eng. Fract. Mech.* 4 (1972) 413–430. doi:10.1016/0013-7944(72)90054-9.

- [89] G.R. Irwin, Linear fracture mechanics, fracture transition, and fracture control, *Eng. Fract. Mech.* 1 (1968) 241–257. doi:10.1016/0013-7944(68)90001-5.
- [90] J.C. Newman, Jr., An evaluation of fracture analysis methods, in: J.C. Newman, Jr., F.J. Loss (Eds.), *ASTM STP 896*, American Society for Testing and Materials, Philadelphia, 1985: pp. 5–96.
- [91] ASTM E1820-18 Standard Test Method for Measurement of Fracture Toughness, in: *ASTM International*, West Conshohocken, PA, 2018.
- [92] P. Lopez-Crespo, S. Pommier, Numerical Analysis of Crack Tip Plasticity and History Effects under Mixed Mode Conditions, *J. Solid Mech. Mater. Eng.* 2 (2008) 1567–1576. doi:10.1299/jmmp.2.1567.
- [93] S. Pommier, P. Lopez-Crespo, P.Y. Decreuse, A multi-scale approach to condense the cyclic elastic-plastic behaviour of the crack tip region into an extended constitutive model, *Fatigue Fract. Eng. Mater. Struct.* 32 (2009) 899–915. doi:10.1111/j.1460-2695.2009.01392.x.

Publications:

1. M. Mokhtarishirazabad, P. Lopez-Crespo, B. Moreno, A. Lopez-Moreno, M. Zanganeh, “Evaluation of crack-tip fields from DIC data: A parametric study”, *International Journal of Fatigue*, Volume 89, 2016, Pages 11-19.

Abstract:

In the past two decades, crack-tip mechanics has been studied increasingly using full-field techniques. Within these techniques, Digital Image Correlation (DIC) has been most widely used due to its many advantages, to extract important crack-tip information, including Stress Intensity Factor (SIF), crack opening displacement, J-integral, T-stress, closure level, plastic zone size, etc. However, little information is given in the literature about the experimental setup that provides best estimations for the different parameters. The current work aims at understanding how the experimental conditions used in DIC influence the crack-tip information extracted experimentally. The influence of parameters such as magnification factor, the position of the images with respect the crack-tip and size of the subset used in the correlation is studied. The influence is studied in terms of SIF by using Williams’ model. In this regard, cyclic loading on a fatigue crack in a compact tension (CT) specimen, made of aluminium 2024-T351 alloy, has been applied and the surface deformation around the crack-tip has been examined. The comparison between nominal and experimental values of KI showed that the effect of subset size on the measured KI is negligible compared to the effect of the field of view and the position of the area of interest.

DOI: <https://doi.org/10.1016/j.ijfatigue.2016.03.006>

2. M. Mokhtarishirazabad, P. Lopez-Crespo, M. Zanganeh, “Stress intensity factor monitoring under cyclic loading by digital image correlation”, *Fatigue Fract. Eng. Mater. Struct.*, Volume 4, 2018, Pages: 2162– 2171.

Abstract:

In the present work, a methodology for structural health monitoring based on a combination of digital image correlation and an analytical elastic solution is presented. To this end, full-field displacement around a crack tip in a CT sample made of 2024-T351 Al alloy under cyclic loading was monitored at different load levels. An analytical solution based on Williams' model was used to evaluate the experimental value of the stress intensity factor (SIF) in a continuous fashion during cyclic loads. It was observed that by increasing the loading amplitude in the cyclic loading, the difference between nominal and experimental estimation of SIF increased due to the crack tip plasticity effect, which was not considered in the nominal evaluations. To consider the plasticity effect, Irwin's approach was employed. The results showed that the proposed method can successfully monitor the evolution of SIF of a sample under cyclic loading until the sudden fracture of the sample.

DOI: <https://doi.org/10.1111/ffe.12825>

3. M. Mokhtarishirazabad, P. Lopez-Crespo, B. Moreno, A. Lopez-Moreno, M. Zanganeh, “Optical and analytical investigation of overloads in biaxial fatigue cracks”, *International Journal of Fatigue*, Volume 100, Part 2, 2017, Pages 583-590.

Abstract:

Structural components are often subjected to complex multiaxial loading conditions. The study of fatigue cracks under such conditions is not easy from an experimental point of view and most works tend to focus more on the simpler but less realistic case of uni-axial loading. Consequently, there are many uncertainties related to the load sequence effect that is now well known and is not normally incorporated into the growth models. The current work presents a new methodology for evaluating overload effect in biaxial fatigue cracks. The methodology includes evaluation of mixed-mode (ΔK_I and ΔK_{II}) stress intensity factor and the Crack Opening Displacement for samples with and without overload cycle under biaxial loading. The methodology is tested under two different load levels and a range of crack lengths. All crack-tip information is obtained with a hybrid optical-analytical methodology. It combines experimental full-field digital image correlation data and Williams' elastic model describing the crack-tip field.

DOI: <https://doi.org/10.1016/j.ijfatigue.2016.12.035>